BRAIN
CLINICAL TRIAL

Spreading depolarizations in ischaemia after subarachnoid haemorrhage, a diagnostic phase III study

Jens P. Dreier,[1,2,3,4,5] Maren K. L. Winkler,[1,6] Sebastian Major,[1,2,3] Viktor Horst,[1] Svetlana Lublinsky,[7,8] Vasilis Kola,[1] Coline L. Lemale,[1,2] Eun-Jeung Kang,[1,2] Anna Maslarova,[9,10] Irmak Salur,[9,11] Janos Lückl,[1,12,13] Johannes Platz,[14] Devi Jorks,[1,4,15] Ana I. Oliveira-Ferreira,[1,16,17,18,19] Karl Schoknecht,[1,20] Clemens Reiffurth,[1,2] Denny Milakara,[1,21] Dirk Wiesenthal,[1,22] Nils Hecht,[1,23] Nora F. Dengler,[1,23] Agustin Liotta,[1,2,24] Stefan Wolf,[1,23] Christina M. Kowoll,[25] André P. Schulte,[26] Edgar Santos,[27] Erdem Güresir,[9] Andreas W. Unterberg,[27] Asita Sarrafzadeh,[28] Oliver W. Sakowitz,[27] Hartmut Vatter,[9] Michael Reiner,[29] Gerrit Brinker,[30] Christian Dohmen,[31] Ilan Shelef,[7,8,32] Georg Bohner,[33] Michael Scheel,[33] Peter Vajkoczy,[1,23] Jed A. Hartings,[34] Alon Friedman,[7,8,35] Peter Martus[36] and Johannes Woitzik[1,37]

Focal brain damage after aneurysmal subarachnoid haemorrhage predominantly results from intracerebral haemorrhage, and early and delayed cerebral ischaemia. The prospective, observational, multicentre, cohort, diagnostic phase III trial, DISCHARGE-1, primarily investigated whether the peak total spreading depolarization-induced depression duration of a recording day during delayed neuromonitoring (delayed depression duration) indicates delayed ipsilateral infarction.

Consecutive patients ($n = 205$) who required neurosurgery were enrolled in six university hospitals from September 2009 to April 2018. Subdural electrodes for electrocorticography were implanted. Participants were excluded on the basis of exclusion criteria, technical problems in data quality, missing neuroimages or patient withdrawal ($n = 25$). Evaluators were blinded to other measures.

Longitudinal MRI, and CT studies if clinically indicated, revealed that 162/180 patients developed focal brain damage during the first 2 weeks. During 4.5 years of cumulative recording, 6777 spreading depolarizations occurred in 161/180 patients and 238 electrographic seizures in 14/180. Ten patients died early; 90/170 developed delayed infarction ipsilateral to the electrodes. Primary objective was to investigate whether a 60-min delayed depression duration cut-off in a 24-h window predicts delayed infarction with >0.60 sensitivity and >0.80 specificity, and to estimate a new cut-off. The 60-min cut-off was too short. Sensitivity was sufficient [= 0.76 (95% confidence interval: 0.65–0.84), $P = 0.0014$] but specificity was 0.59 (0.47–0.70), i.e. <0.80 ($P < 0.0001$). Nevertheless, the area under the receiver operating characteristic (AUROC) curve of delayed depression duration was 0.76 (0.69–0.83, $P < 0.0001$) for delayed infarction and 0.88 (0.81–0.94, $P < 0.0001$) for delayed ischaemia (reversible delayed neurological deficit or infarction). In secondary analysis, a new 180-min cut-off indicated delayed infarction with a targeted 0.62 sensitivity and 0.83 specificity. In awake patients, the AUROC curve of delayed depression duration was 0.84 (0.70–0.97, $P = 0.001$) and the prespecified 60-min cut-off showed 0.71 sensitivity and 0.82 specificity for reversible neurological deficits. In multivariate analysis, delayed depression duration ($\beta = 0.474$, $P < 0.001$), delayed median Glasgow Coma Score ($\beta = -0.201$, $P = 0.005$) and peak transcranial Doppler ($\beta = 0.169$, $P = 0.016$) explained 35% of variance in delayed infarction. Another key finding

Received May 11, 2021. Revised August 18, 2021. Accepted November 21, 2021. Advance access publication April 12, 2022

was that spreading depolarization-variables were included in every multiple regression model of early, delayed and total brain damage, patient outcome and death, strongly suggesting that they are an independent biomarker of progressive brain injury.

While the 60-min cut-off of cumulative depression in a 24-h window indicated reversible delayed neurological deficit, only a 180-min cut-off indicated new infarction with >0.60 sensitivity and >0.80 specificity. Although spontaneous resolution of the neurological deficit is still possible, we recommend initiating rescue treatment at the 60-min rather than the 180-min cut-off if progression of injury to infarction is to be prevented.

1 Centre for Stroke Research Berlin, Charité – Universitätsmedizin Berlin, Corporate Member of Freie Universität Berlin, Humboldt-Universität zu Berlin, and Berlin Institute of Health, Berlin, Germany
2 Department of Experimental Neurology, Charité – Universitätsmedizin Berlin, Corporate Member of Freie Universität Berlin, Humboldt-Universität zu Berlin, and Berlin Institute of Health, Berlin, Germany
3 Department of Neurology, Charité – Universitätsmedizin Berlin, Corporate Member of Freie Universität Berlin, Humboldt-Universität zu Berlin, and Berlin Institute of Health, Berlin, Germany
4 Bernstein Centre for Computational Neuroscience Berlin, Berlin, Germany
5 Einstein Centre for Neurosciences Berlin, Berlin, Germany
6 Robert Koch-Institute, Berlin, Germany
7 Department of Brain & Cognitive Sciences, Zlotowski Centre for Neuroscience, Faculty of Health Sciences, Ben-Gurion University of the Negev, Soroka University Medical Centre, Beer-Sheva, Israel
8 Department of Physiology & Cell Biology, Zlotowski Centre for Neuroscience, Faculty of Health Sciences, Ben-Gurion University of the Negev, Soroka University Medical Centre, Beer-Sheva, Israel
9 Department of Neurosurgery, University Hospital and Friedrich-Wilhelms-University Bonn, Bonn, Germany
10 Department of Neurosurgery, Universitätsklinikum Erlangen, Friedrich-Alexander University Erlangen-Nürnberg, Erlangen, Germany
11 Department of Neurosurgery, KRH Klinikum Nordstadt, Hannover, Germany
12 Department of Medical Physics and Informatics, University of Szeged, Szeged, Hungary
13 Department of Neurology, University of Szeged, Szeged, Hungary
14 Department of Neurosurgery, Herz-Neuro-Zentrum Bodensee, Kreuzlingen, Switzerland
15 Clienia Schlössli AG, Privatklinik für Psychiatrie und Psychotherapie, Oetwil am See, Switzerland
16 Neuro-Electronics Research Flanders, Leuven, Belgium
17 VIB-KU, Leuven, Belgium
18 Interuniversity Microelectronics Centre, Leuven, Belgium
19 Laboratory of Neural Circuits, Department of Neurosciences, KU Leuven, Leuven, Belgium
20 Carl Ludwig Institute for Physiology, Medical Faculty, University of Leipzig, Leipzig, Germany
21 Research Campus STIMULATE, Otto-von-Guericke-University, Magdeburg, Germany
22 Univention GmbH, Bremen, Germany
23 Department of Neurosurgery, Charité – Universitätsmedizin Berlin, Corporate Member of Freie Universität Berlin, Humboldt-Universität zu Berlin, and Berlin Institute of Health, Berlin, Germany
24 Department of Anaesthesiology and Intensive Care, Charité – Universitätsmedizin Berlin, Corporate Member of Freie Universität Berlin, Humboldt-Universität zu Berlin, and Berlin Institute of Health, Berlin, Germany
25 Department of Neurology, University of Cologne, Faculty of Medicine and University Hospital Cologne, Cologne, Germany
26 Department of Spinal Surgery, Krankenhaus der Augustinerinnen, Cologne, Germany
27 Department of Neurosurgery, Heidelberg University Hospital, Ruprecht-Karls-University Heidelberg, Germany
28 Division of Neurosurgery, Department of Clinical Neurosciences, Faculty of Medicine, Geneva University Medical Centre, Geneva, Switzerland
29 Medical Advisory Service of the Statutory Health Insurance of North Rhine, Germany
30 Department of Neurosurgery, University of Cologne, Faculty of Medicine and University Hospital Cologne, Cologne, Germany
31 Department for Neurology and Neurological Intensive Care Medicine, LVR-Klinik Bonn, Bonn, Germany
32 Institute of Radiology, Soroka University Medical Centre, Beer-Sheva, Israel
33 Department of Neuroradiology, Charité – Universitätsmedizin Berlin, Corporate Member of Freie Universität Berlin, Humboldt-Universität zu Berlin, and Berlin Institute of Health, Berlin, Germany
34 Department of Neurosurgery, University of Cincinnati College of Medicine, Cincinnati, OH, USA
35 Department of Medical Neuroscience and Brain Repair Centre, Dalhousie University, Halifax, Nova Scotia, Canada
36 Institute for Clinical Epidemiology and Applied Biometry, University of Tübingen, Tübingen, Germany
37 Department of Neurosurgery, Evangelisches Krankenhaus Oldenburg, University of Oldenburg, Oldenburg, Germany

Correspondence to: Jens P. Dreier
Centre for Stroke Research
Campus Charité Mitte
Charité – Universitätsmedizin Berlin
Charitéplatz 1, 10117 Berlin, Germany
E-mail: jens.dreier@charite.de

Keywords: cytotoxic oedema; spreading depolarization; spreading ischaemia; subarachnoid haemorrhage; vasospasm

Abbreviations: ABT = abnormal brain tissue; aSAH = aneurysmal subarachnoid haemorrhage; DCI = delayed cerebral ischaemia; DND = delayed neurological deficit; DISCHARGE-1 = depolarizations in ischaemia after subarachnoid haemorrhage-1; DSAS = digital subtraction angiography score; ECI = early cerebral ischaemia; ECoG = electrocorticography; (e)GOS = (extended) Glasgow Outcome Score; ICH = intracerebral haemorrhage; ICP = intracranial pressure; MAP = mean arterial (blood) pressure; mbfv = mean blood flow velocity; MCA = middle cerebral artery; MWRST = Mann–Whitney rank sum test; NUP = negative ultraslow potential; PTDDD = peak total spreading depolarization-induced depression duration of a recording day; RMS = Rosen–Macdonald score; SD = spreading depolarization; TCD = transcranial Doppler sonography; TDDD = total (cumulative) SD-induced depression duration; WFNS = World Federation of Neurosurgical Societies score

Introduction

Aneurysmal subarachnoid haemorrhage (aSAH) is the second most frequent type of haemorrhagic stroke.[1,2] Most prominent aetiologies of focal brain damage associated with aSAH are intracerebral haemorrhage (ICH),[3,4] and infarction due to either early cerebral ischaemia (ECI),[5,6] or delayed cerebral ischaemia (DCI).[7–10] Delayed infarcts are those that develop >2 days after the initial haemorrhage. DCI is thus a potentially modifiable aetiology of focal brain damage during neurocritical care, as it allows treatment of patients with a neuroprotective intervention before the possible insult or shortly thereafter. The risk of DCI is particularly high after severe aSAH. Severe cases require mechanical ventilation and sedation more often, which limits neurological assessment. Therefore, in the high-risk population, it is particularly difficult to identify and treat those patients who suffer from the complication. However, neurosurgical procedures are indicated early after aSAH, allowing implantation of invasive probes. This enables recording of the entire period of ischaemic stroke development, early treatment stratification according to changes in diagnostic summary measures recorded by neuromonitoring devices in real time and then reassessment of these measures after neuroprotective interventions.[11]

In animals, spreading depolarization (SD) is the electrophysiological correlate of the initial, still-reversible phase of neuronal cytotoxic oedema in the cerebral grey matter.[12–19] SD is imaged experimentally as a wave of diffusion restriction with MRI [diffusion-weighted images (DWI)–MRI] or neuronal swelling with two-photon microscopy.[15,16,20–22] Neurons die if depolarization and cytotoxic oedema persist, as determined by a negative ultraslow potential (NUP) in electrophysiology and continued diffusion restriction in DWI–MRI.[4,6,8,11] Therefore, it has been suggested that SD may serve as a real-time mechanistic biomarker for impending parenchyma damage after aSAH.[11,23–25]

In patients and animals, SD is observed as a large negative direct current (DC)-electrocorticography (ECoG) shift that spreads between adjacent recording sites (Fig. 1B).[11] In contrast, SD-induced spreading depression of spontaneous activity is observed as a rapidly evolving reduction in amplitudes in alternating current-ECoG recordings (Fig. 1B).[26,27]

Primary objective of the prospective, observational, multicentre, cohort, diagnostic phase III trial 'Depolarizations in ischaemia after subarachnoid haemorrhage-1' (DISCHARGE-1) was to calculate: (i) sensitivity; and (ii) specificity for a known cut-off value for the peak total SD-induced depression duration of a recording day (PTDDD) during the delayed neuromonitoring period ($PTDDD_{delayed}$) that indicates delayed ischaemic infarcts ipsilateral to the recording strip as assessed by serial neuroimaging; and (iii) to estimate a new cut-off value. As formulated *a priori* (https://doi.org/10.1186/ISRCTN05667702) and explained in detail in the published recommendations of the Co-Operative Studies on Brain Injury Depolarizations (COSBID) (https://www.cosbid.org/) on recording and analysis of SDs,[26] the concept of this approach is that a yet-to-be developed automated detection system will in the future trigger an alarm as soon as the cumulative SD-induced depression duration in the sliding window of the just-past 24-h period exceeds a cut-off to initiate treatment before the injury has progressed to infarction. Secondary outcome measures in DISCHARGE-1 were: (i) occurrence of delayed neurological deficit (DND) in clinically assessable, non-sedated patients; (ii) manually segmented volumes of ipsilateral damage due to ICH, ECI and DCI alone, or in combination; (iii) semi-automatically segmented ipsilateral abnormal brain tissue (ABT) (reflecting cytotoxic or vasogenic oedema, gliosis or haemorrhage) as a percentage of ipsilateral brain volume in early MRIs ($ABT\%_{early}$) and MRIs after neuromonitoring ($ABT\%_{Day14}$); (iv) extended Glasgow Outcome Score (eGOS) at 7 months; and (v) death to follow-up. We also performed secondary multivariate analyses whether: (i) variables of the early neuromonitoring period were associated with the volume of early focal brain damage; (ii) variables of the delayed period—including daily transcranial Doppler (TCD) and delayed digital subtraction angiography (DSA)—with delayed damage; and (iii) variables of the entire neuromonitoring period with total brain damage. In further analysis, we used stepwise prognostic models to determine the impact of the different variables on patient outcome at 7 months. Young age and severe complications make aSAH one of the leading causes of brain death worldwide.[28] The relative youth of the affected individuals means that aSAH is responsible for a quarter of all years of life lost due to stroke.[29] Therefore, we also investigated potential predictors of (i) early in-hospital death; and (ii) delayed death. All of these secondary analyses

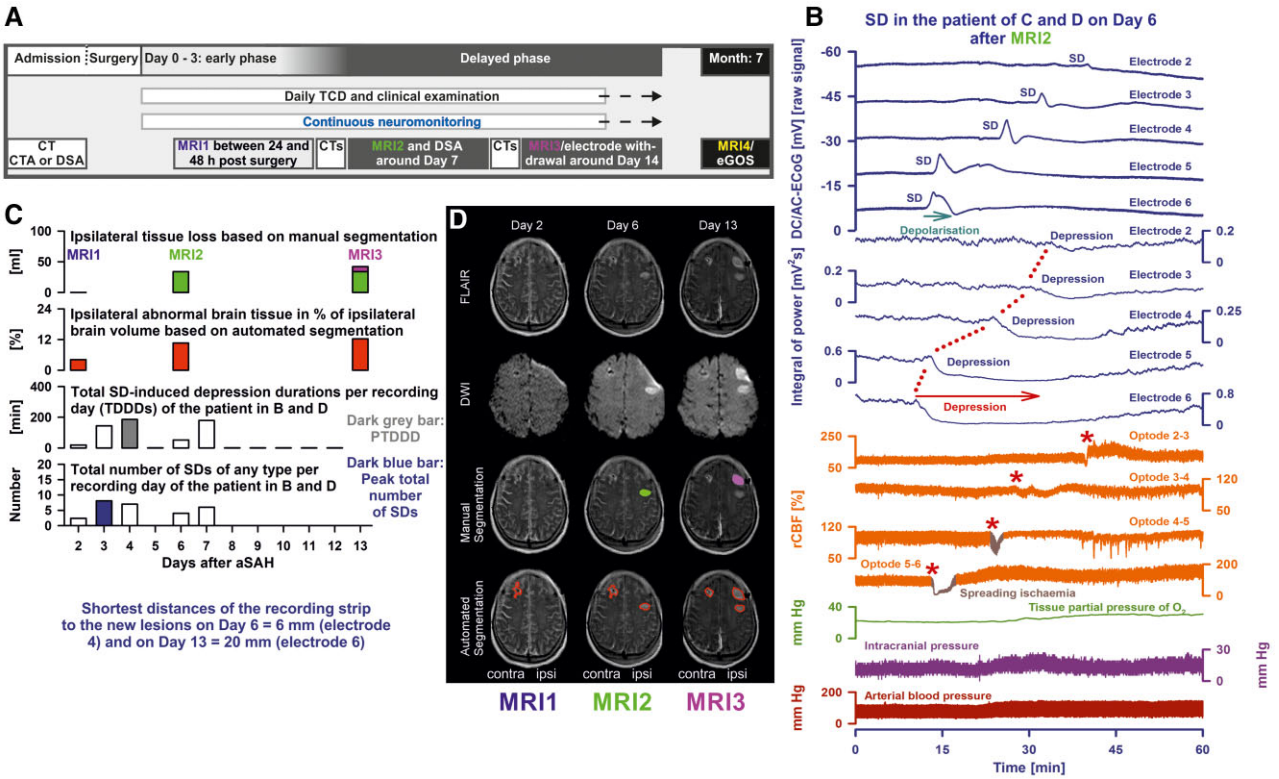

Figure 1 Methodological approach that allowed the correlation of SD variables with parenchymal damage volumes. (**A**) Study flow chart. CTA = CT angiography; DSA = digital subtraction angiography; eGOS = extended Glasgow Outcome Score; TCD = transcranial Doppler sonography. (**B**) Example SD. Traces 1–5 from *top* to *bottom* give the DC/AC-ECoG recordings (band-pass: 0–45 Hz). SD is observed as a negative DC shift (green arrow in trace 5) propagating across the cortex from electrode 6 to electrode 2. Traces 6–10 reveal the depressive effect of the SD on the spontaneous activity as assessed in the high-frequency band between 0.5 and 45 Hz using the integral of the total power of the band-pass filtered data.[26] The duration of the depression period was scored beginning at the initial decrease in the integral of power and ending at the start of the recovery phase (red arrow).[25,26] Traces 11–14 give regional cerebral blood flow (rCBF) recorded with four optodes between the five electrodes. SD is known to induce tone alterations in resistance vessels (red asterisks), causing either transient hyperperfusion (physiological haemodynamic response) in healthy tissue; or initial hypoperfusion [inverse haemodynamic response = spreading ischaemia (marked in grey)] in tissue where the neurovascular unit is disturbed.[8,11,55] Trace 15: tissue partial pressure of oxygen measured with an intraparenchymal oxygen sensor close to optode 3–4. Trace 16: intracranial pressure [measured via extraventricular drainage (EVD) catheter]. Trace 17: systemic arterial pressure (measured via radial artery catheter). (**C**) Time course of SD variables and focal brain damage in the same patient as in **B**. *Row 1* in **C** shows the progression of focal brain damage from MRI1 to MRI2 to MRI3 based on manual neuroimage segmentation of the hemisphere ipsilateral to the recording strip. MRI3 was performed after the end of neuromonitoring. *Row 2* shows abnormal brain tissue (ABT) ipsilateral to the recording strip as a percentage of ipsilateral brain volume (ABT%) based on semi-automated neuroimage segmentation of MRI1, MRI2 and MRI3. $ABT\%_{early}$: ABT% of the early MRI (MRI1), $ABT\%_{Day14}$: ABT% of the MRI after the end of neuromonitoring (MRI3). *Rows 3* and *4*: For each day, SDs were counted and depression durations were scored to determine the total duration of SD-induced activity depression per recording day (TDDD) (*row 3*) and the total number of SDs per recording day (*row 4*). The peak TDDD (PTDDD) and peak SDs/day ($peak_{SD}$) were defined for each patient as the maximal values among all recording days (indicated with a dark grey and dark blue bar, respectively). (**D**) Longitudinal MRIs of the same patient as in **B** and **C** are presented at the level of the centrum semi-ovale. MRI1 showed neither ICH nor focal damage due to ECI. Fluid attenuation inversion recovery (FLAIR) images (*row 1*) showed only a hyperintense rim around an EVD catheter contralateral to the recording strip, consistent with vasogenic oedema. MRI2 revealed a hyperintense lesion on FLAIR (*row 1*) and DWI (*row 2*) in the left frontal cortex indicating a delayed infarct ipsilateral to the recording strip. Another delayed infarct was found in MRI3 on Day 13. Marked in green and purple, *row 3* shows the ipsilateral focal damage due to DCI based on manual neuroimage segmentation. Bordered in red, *row 4* shows ABT based on semi-automated neuroimage segmentation.

addressed the same fundamental hypothesis of whether SD variables are an independent biomarker of progressive brain injury and whether this is true for all conditions and time windows studied.

Materials and methods

Standard protocol approvals, registrations and patient consent

Patients with aSAH were screened for study inclusion and were consecutively enrolled in DISCHARGE-1 at six university hospitals [Campus Benjamin Franklin ($n = 66$) and Campus Virchow Klinikum ($n = 61$), Charité-Universitätsmedizin Berlin; University of Bonn ($n = 26$); Goethe-University Frankfurt ($n = 23$); University of Cologne ($n = 16$) and University Hospital Heidelberg ($n = 13$)] between September 2009 and April 2018 (Supplementary Fig. 1). Five out of 205 patients were excluded based on exclusion criteria (Supplementary material and Supplementary Fig. 2). Twenty of the remaining 200 participants were excluded from analysis because of technical problems in data quality, missing neuroimages or patient withdrawal (Supplementary material and Supplementary Fig. 2). The protocol was approved by the local

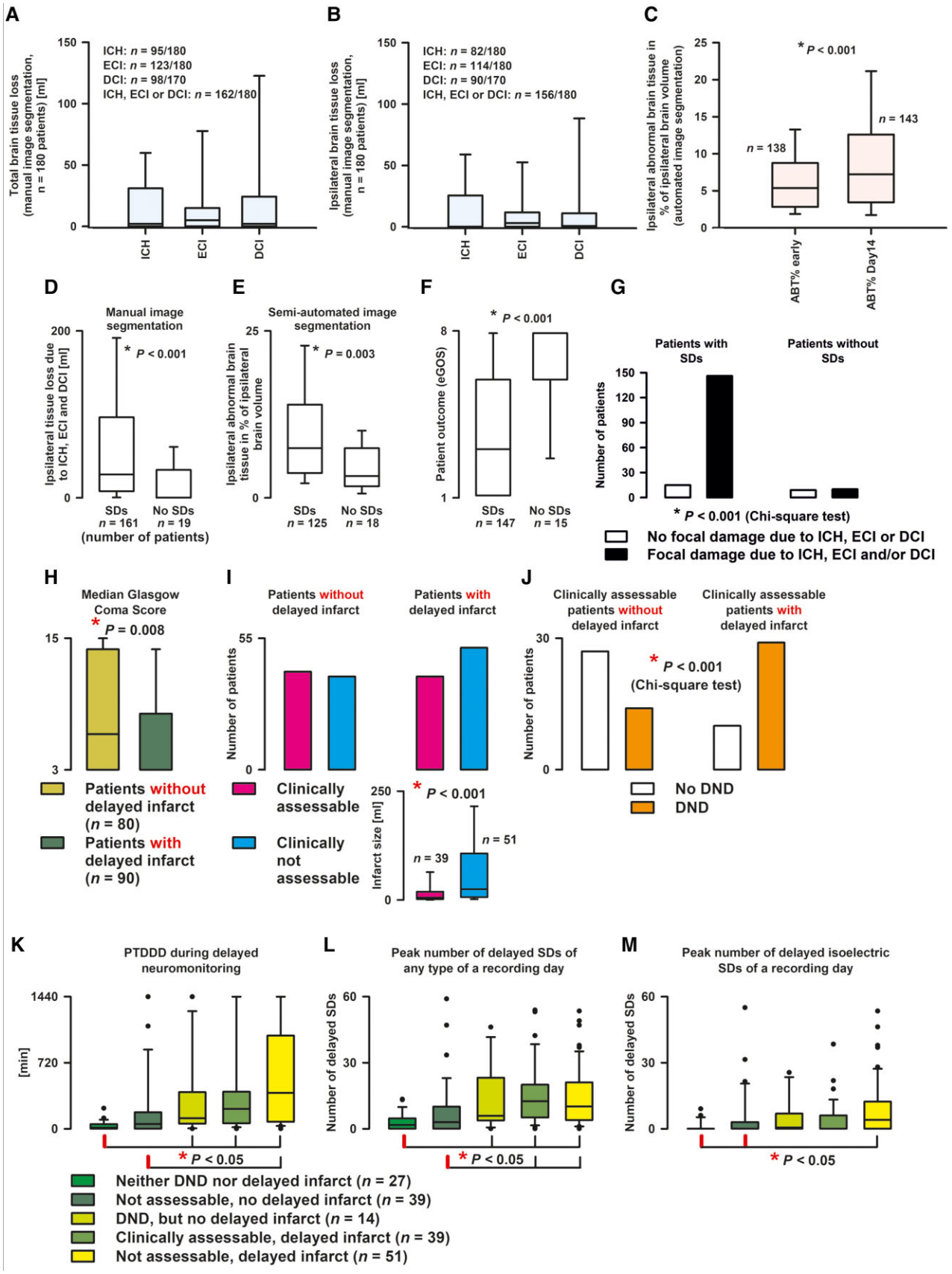

Figure 2 Description of the study population—first part. (**A**) Manually segmented volumes of focal brain damage due to ICH, ECI and DCI. For this comparison, ipsilateral and contralateral cerebral hemisphere and infratentorial brain including brainstem and cerebellum were considered.

(Continued)

ethics committees of all participating universities. Either informed consent or surrogate informed consent was obtained. Research was conducted in accordance with the Declaration of Helsinki. Results are reported in accordance with the Strengthening the Reporting of Observational Studies in Epidemiology guidelines (https://www.strobe-statement.org/). DISCHARGE-1 was preregistered at the ISCRTN registry (https://doi.org/10.1186/ISRCTN05667702). Minor deviations from the preregistration are explained in the Supplementary material.

Study flow, recording, analysis and neuroimaging

Figure 1A shows the study flow. Inclusion and exclusion criteria are given in the Supplementary material. Study protocol, clinical scores and definitions, neuroimaging and neuromonitoring are described in the Supplementary material. Recording, analysis and interpretation of SDs followed the published recommendations of the COSBID group.[26] Importantly, in every patient, the first 24-h period after the initial haemorrhage was always denoted as 'Day 0', the second 24-h period as 'Day 1' and so on. Figure 1C illustrates the approach that allowed correlation of SD variables with parenchymal damage volumes. In brief, for each recording day of each patient, we determined the following: (i) total (cumulative) SD-induced depression duration (TDDD); (ii) number of SDs; (iii) number of SDs in electrically inactive tissue (isoelectric SDs)[26,30]; and (iv) number of clustered SDs, i.e. SDs that occurred <1 h apart from the previous SD. Supplementary Fig. 3 shows the overall time courses of TDDDs, number of SDs, number of isoelectric SDs and number of clustered SDs for each 24-h period from Days 0 to 14 after the initial haemorrhage. In total, 2017 24-h periods at a sampling rate of 200 Hz were available in the 180 patients for which the four SD variables could be determined. In every patient, we then determined peak values of a recording day for each SD-variable resulting in (i) PTDDD; (ii) peak number of SDs of any type ($peak_{SD}$); (iii) peak number of isoelectric SDs ($peak_{isoSD}$); and (iv) peak number of clustered SDs ($peak_{clusSD}$). This was done for three predefined periods: (i) the early period (Days 0–3 after the initial haemorrhage); (ii) the delayed period between the early neuroimage on Day 2 (median) [interquartile range (IQR): Days 1–3] and the neuroimage after the end of neuromonitoring on Day 14 (IQR: 13–16); and (iii) the entire neuromonitoring period. Neuromonitoring time was similar between patients with and without delayed infarction [231.1 h (IQR: 192.3–270.1, $n = 90$) versus 233.7 h (IQR: 188.6–277.8, $n = 80$), $P = 0.458$, Mann–Whitney rank sum test (MWRST)].

Parenchymal damage volumes were determined via either manual or semi-automated neuroimage segmentation as shown in Fig. 1D (Supplementary material). Manual segmentation allowed us to analyse both MRIs and CTs and determine damage volumes separately by ICH, ECI or DCI. Volumes of ICH and ECI were added together to obtain tissue loss due to early focal brain injury. Tissue loss due to DCI was defined as new damage in the neuroimage after neuromonitoring compared to the pre-existing damage in the early neuroimage. Total tissue loss resulted from ICH + ECI + DCI. Manually segmented volumes of focal brain damage due to ICH, ECI and DCI are compared in Fig. 2A. For this comparison, ipsilateral and contralateral cerebral hemisphere and infratentorial brain including brainstem and cerebellum were considered. Hereafter, we only considered supratentorial parenchymal damage ipsilateral to the recording strip to investigate the possible association between manually or semi-automatically segmented brain damage and SD variables, as SDs do not spread to the contralateral hemisphere (Figs 2B and C).

Statistical analysis

The primary hypothesis was that a predefined 60-min cut-off for $PTDDD_{delayed}$ predicts delayed infarction with sensitivity >0.60 and specificity >0.80. The choice of the cut-off was based on a pilot

Figure 2 Continued
The volumes between these three most prominent aetiologies of focal brain damage after aSAH did not differ significantly. In the *top left corner*, the number of affected patients out of the total number of patients analysed is indicated. Ten patients died before the first follow-up image. Therefore, the occurrence of DCI could only be investigated in 170 patients. On average, the patient admitted to the neurocritical care unit after aneurysm treatment had already lost 46.3 ± 72.6 ml of brain tissue and lost an additional 36.3 ± 80.1 ml over the next 2 weeks. (**B**) Manually segmented volumes of focal brain damage due to ICH, ECI and DCI in the hemisphere ipsilateral to the subdural recording strip. No significant differences were found between ICH, ECI and DCI. (**C**) Ipsilateral abnormal brain tissue as a percentage of ipsilateral brain volume (ABT%) based on semi-automated segmentation of the early MRI ($ABT\%_{early}$) is compared with ABT% of the MRI after the end of neuromonitoring ($ABT\%_{Day14}$). $ABT\%_{Day14}$ was significantly >$ABT\%_{early}$ (Wilcoxon signed rank test, $n = 137$). This is conclusively explained by the appearance of new lesions due to DCI. (**D**) Comparison of the manually segmented ipsilateral ICH + ECI + DCI damage between patients with and without SDs (MWRST). (**E**) Comparison of ipsilateral $ABT\%_{Day14}$ between patients with and without SDs (MWRST). (**F**) Comparison of patient outcome (eGOS) at 7 months between patients with and without SDs (MWRST). (**G**) Patients with at least one SD were significantly more likely to show ipsilateral focal brain damage than patients without SD. (**H**) Patients with delayed infarction showed a lower median GCS during neuromonitoring than patients without delayed infarction (MWRST). (**I**) Overall, only 80/170 (47.1%) patients were clinically assessable in the delayed phase (*top* graph). The *bottom* graph in **I** shows that within the group of delayed infarction patients, clinically non-assessable patients had significantly greater delayed infarct volume than clinically assessable patients (MWRST). (**J**) Clinically assessable patients with delayed infarction were more likely to show a DND than patients without delayed infarction. However, in about one-third of cases, DNDs were completely reversible, that is, they corresponded by definition to a transitory ischaemic attack. (**K**) Patients with delayed cerebral ischaemia (DCI: DND and/or delayed ipsilateral infarction) showed a higher PTDDD during the delayed period ($PTDDD_{delayed}$) than clinically assessable patients without DCI. In addition, non-assessable patients with delayed infarction showed a higher $PTDDD_{delayed}$ than non-assessable patients without delayed infarction. (**L**) Patients with DCI also had a higher peak number of SDs of a recording day ($peak_{SD}$) during the delayed period than clinically assessable patients without DCI. Further, non-assessable patients with delayed infarction showed higher $peak_{SD\text{-}delayed}$ than non-assessable patients without delayed infarction. (**M**) Non-assessable patients with delayed infarction also showed a higher peak number of isoelectric SDs of a recording day ($peak_{isoSD}$) during the delayed period than non-assessable patients without delayed infarction. In **K–M**, Kruskal–Wallis one-way ANOVA on ranks with *post hoc* Dunn's tests were performed. All image-based information in **B–M** refers to the side ipsilateral to the recording strip. However, the 41 clinically assessable patients without delayed infarction also did not develop delayed infarction in the contralateral hemisphere or infratentorially. Note that the GCS documentation was insufficient in 14/170 (8.2%) patients. In the figure shown here, these patients were included in the group of patients who could not be clinically assessed. We also performed the same tests after excluding these patients without any relevant changes in the results. The whiskers (error bars) above and below the boxes indicate the 90th and 10th percentiles.

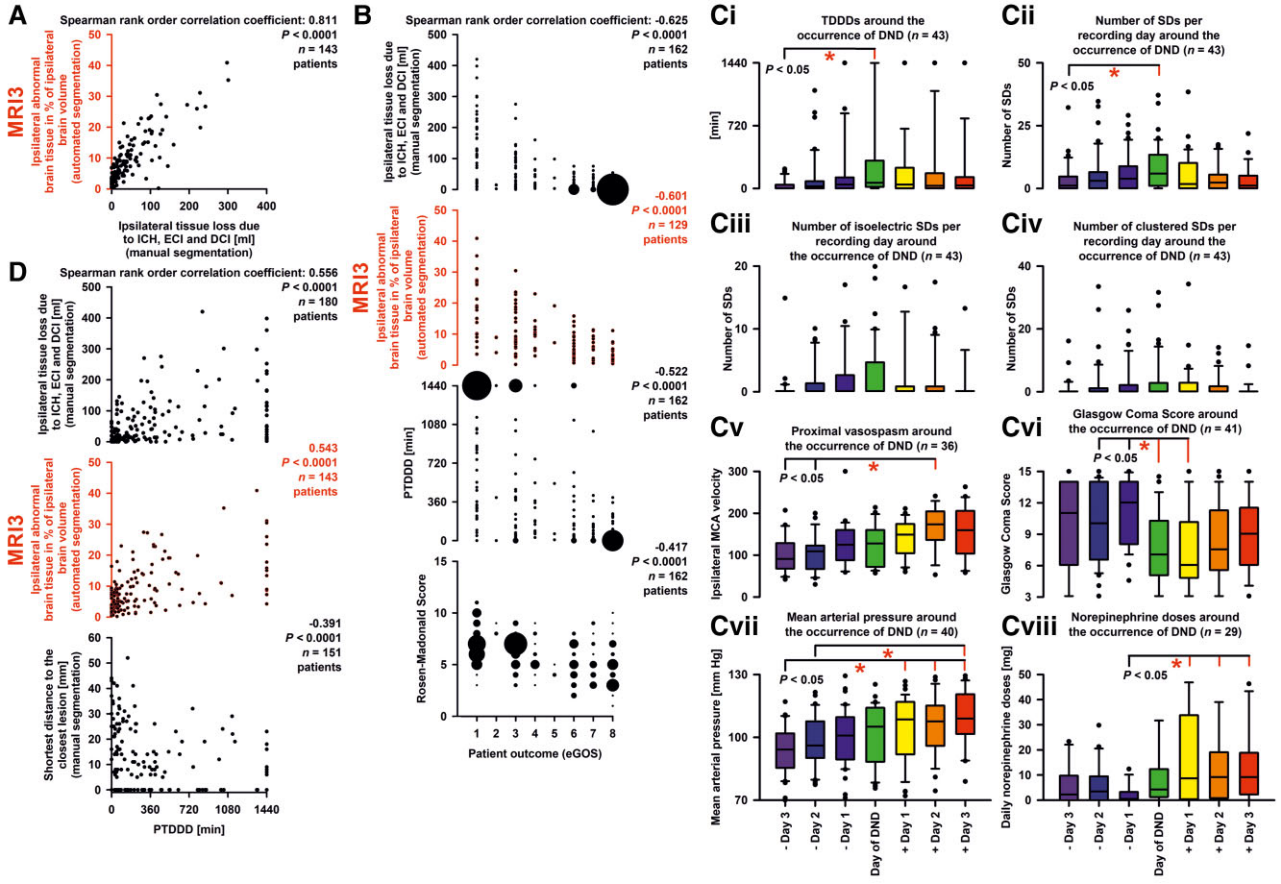

Figure 3 Description of the study population—second part. (**A**) Semi-automatically segmented ipsilateral abnormal brain tissue as a percentage of ipsilateral brain volume of the MRI after the end of neuromonitoring (= ABT%$_{Day14}$, *y*-axis) strongly correlated with the manually segmented ipsilateral focal brain damage due to ICH, ECI and DCI (*x*-axis). (**B**) Patient outcome (eGOS) at 7 months (*y*-axis) correlated negatively with ICH + ECI + DCI damage, ABT%$_{Day14}$, PTDDD during the entire period (PTDDD$_{entire}$) and RMS. The correlations of eGOS with ICH + ECI + DCI damage, PTDDD$_{entire}$ and RMS are presented using bubble plots to account for the fact that the same pairs of values could occur more than once and then received more weight. (**C**) DND were detected in 43/80 (53.8%) clinically assessable patients. The plots show the time course of the different variables in a period of 3 days before and 3 days after the occurrence of the DND, respectively (*x*-axes of the two *bottom* plotsalso apply to the *top* plots). Kruskal–Wallis one-way ANOVA on ranks with *post hoc* Dunn's tests were performed. The 'ipsilateral MCA velocity' is the mbfv measured with TCD. MAP was recorded with a catheter in the radial artery. In particular, it can be seen in **C** (**vii** and **viii**) that the significant increase in norepinephrine doses for hyperdynamic therapy and the increase in MAP began only after the onset of DND and the peak of the SD variables shown in **C(i–iv)**, respectively. This suggests that hyperdynamic therapy started too late to significantly influence the test sensitivity and specificity of the SD variables. In addition, it is seen that the time course of the SD variables correlated better with the DND-associated drop in GCS than the TCD-determined mbfvs. (**D**) Correlations of the most important neuroimaging variables, ICH + ECI + DCI damage and ABT%$_{Day14}$ (*y*-axes) with PTDDD$_{entire}$ (*x*-axis). While the two *top* plots demonstrate that the PTDDD$_{entire}$ correlated positively with both types of damage volume, the *bottom* plot shows that it correlated negatively with the shortest distance to the nearest lesion. In other words, the predictive value of neuromonitoring was influenced not only by the size of an emerging lesion but also by the distance of the electrode strip from the lesion. Conversely, the bottom plot confirms that regional electrocorticographic monitoring afforded even remote detection of injury because SDs propagate widely from metabolically stressed zones.[26] When interpreting electrocorticographic patterns, it is important to keep in mind that the patterns change along a continuum with distance from the developing lesion, as explained previously,[8,50] and illustrated in Figs 4 and 5.

study from 2006,[25] in which a sensitivity and specificity of 1.0 each was found for this cut-off ($n = 18$). For sample size estimation, a true sensitivity of 0.85 and a true specificity of 0.90 was assumed, and the type 1 error was set to 0.025 two-sided to respect multiplicity of testing sensitivity and specificity. The aim was to allocate 200 patients to trial, of whom 160 would be analysable. On the basis of 4/18 (22.2%) patients with delayed infarction in the pilot study,[25] delayed infarction was expected in 20% of patients. Additionally, receiver operating characteristic (ROC) analysis was performed to investigate the *a priori* defined primary study objective and new cut-offs were derived in an exploratory manner. We also explored the study population regarding the predefined secondary outcome measures, including multivariate association and prognostic analyses.

Two-group comparisons were made using the Mann–Whitney rank sum test. For statistical analysis in the figures illustrating the relationships between untransformed variables, we used Spearman rank order correlations of the non-log transformed data. Comparisons between several groups were done using parametric methods for continuous variables (ANOVA), and Kruskal–Wallis test, if normal distribution could not be confirmed.

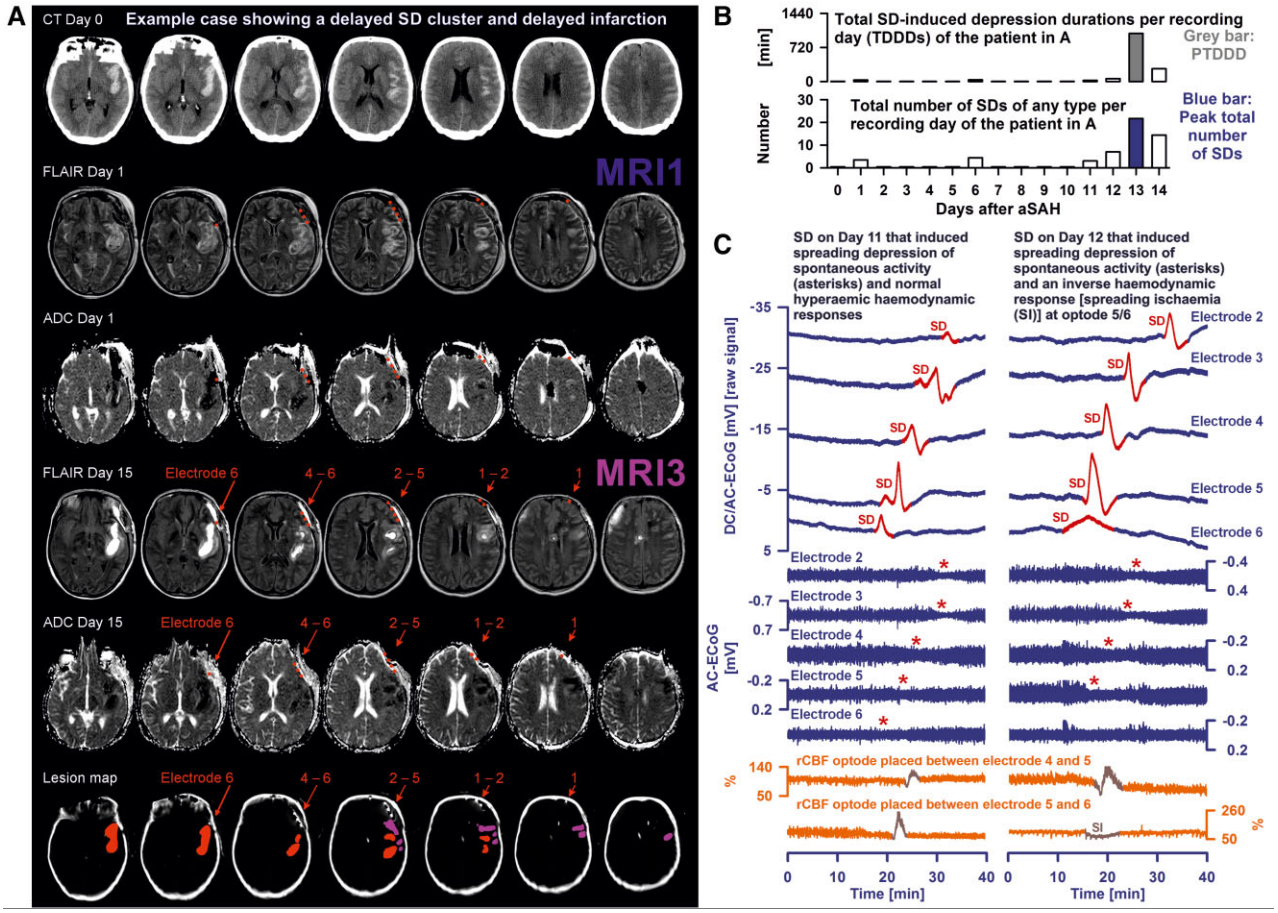

Figure 4 Example case of delayed infarction—first part. Example case illustrating the assessment of focal brain damage using serial MRI scans (**A**), a SD cluster associated with delayed cerebral infarction (**B**) and the changes in haemodynamic responses to SD over time prior to infarction (**C**). (**A**) Representative CT and MRI slices in axial orientation in a patient with rupture of an aneurysm of the left MCA. All images were aligned to the first postoperative T_1 spin echo scan (6 mm slice thickness). The initial CT scan on admission showed the SAH and a large clot in the left lateral Sylvian fissure. The clot extended into the inferoposterior temporal parenchyma. This intraparenchymal bleeding was rated as ICH (volume: 19 ml). The first postoperative MRI scan (MRI1) 27 h after the initial haemorrhage reveals a hyperintense rim around the blood clot on FLAIR images with restricted diffusion on the apparent diffusion coefficient (ADC) map. These findings are consistent with perihaematomal oedema. Electrodes (marked in red) were projected from the postoperative CT scan on Day 9 onto the MRI scan. MRI2 on Day 8 did not reveal significant changes, in particular no signs of delayed cerebral infarction (images not shown). MRI3 on Day 15 demonstrated a new cortical infarct close to the left-sided haematoma (hyperintense in FLAIR images and hypointense in the ADC map, volume: 5 ml). The delayed infarct was confined to cortical grey matter of the left anterior ascending ramus, where electrodes 5 and 6 were placed, the left precentral sulcus and the inferior portion of the left central sulcus. The *bottom row* shows the CT on Day 9 with the platinum-iridium electrodes as hyperdense points in the subdural space and the quantified lesions from these scans projected onto the CT. The red-labelled area indicates the blood clot in the Sylvian fissure with intracerebral extensions, the pink area the delayed infarct in MRI3 on Day 15. (**B**) SDs were counted and depression durations were scored for each day to determine the TDDD (*top* plot), and the total number of SDs per recording day (*bottom* plot). The PTDDD and peak SDs/day ($peak_{SD}$) were defined as the maximal values among all recording days (indicated with a dark grey and dark blue bar, respectively). The patient developed a delayed SD cluster that began gradually on Day 11 and peaked on Day 13. (**C**) Traces 1–5 from *top* to *bottom* give the raw DC/AC-ECoG recordings (band-pass: 0–45 Hz) showing the propagation of the negative DC shifts across the cortex from electrode 6 to electrode 2. Traces 6–10 reveal the depressive effect of the two SDs on the spontaneous activity as assessed in the higher frequency band between 0.5 and 45 Hz. Traces 11 and 12 give regional cerebral blood flow (rCBF) recorded with two optodes, one between electrodes 4 and 5 (trace 11) and the other one between electrodes 5 and 6 (trace 12). In the *left* part, one of the single SDs on Day 11, and in the *right* part, one of the single SDs on Day 12 is displayed. SD characteristics on Day 11 indicate that the recording site is essentially still metabolically intact. Thus, (i) negative DC shifts are short-lasting and followed by positive shifts; (ii) SD-induced depression periods are short-lasting; and (iii) haemodynamic responses (marked in grey) are characterized by predominant hyperaemia. In contrast, SD characteristics on Day 12 indicate progressive disruption of the neurovascular unit at optode 5/6 (trace 12). Thus, the previously almost normal hyperaemic response has now changed to a slightly inverse response.[11] The resulting local energy deficiency causes a characteristic prolongation of the negative DC shift at electrode 6 and to a lesser extent at electrode 5. Because the negative DC shifts are prolonged, the haemodynamic response to SD at optode 5/6 on Day 12 fulfils the criteria of a spreading ischaemia (SI).[11,55,64] Before the detection of the new infarct at electrodes 5 and 6 in MRI3 on Day 15 (**A**), the patient showed further progression to severe and very long-lasting spreading ischaemia at optode 5/6 on Day 13. These recordings are displayed in Fig. 5.

Chi-square tests were done for comparing categorical variables between groups.

In the association and the prognostic part, DSA score (DSAS),[31] each of the SD variables, ipsilateral tissue losses based on manual neuroimage segmentation and ABT% variables were submitted to logarithmic transformation to approach normal distribution. The hypothesis 'SD variables correlate to parenchyma damage after aSAH' was analysed by use of Pearson correlation analysis and

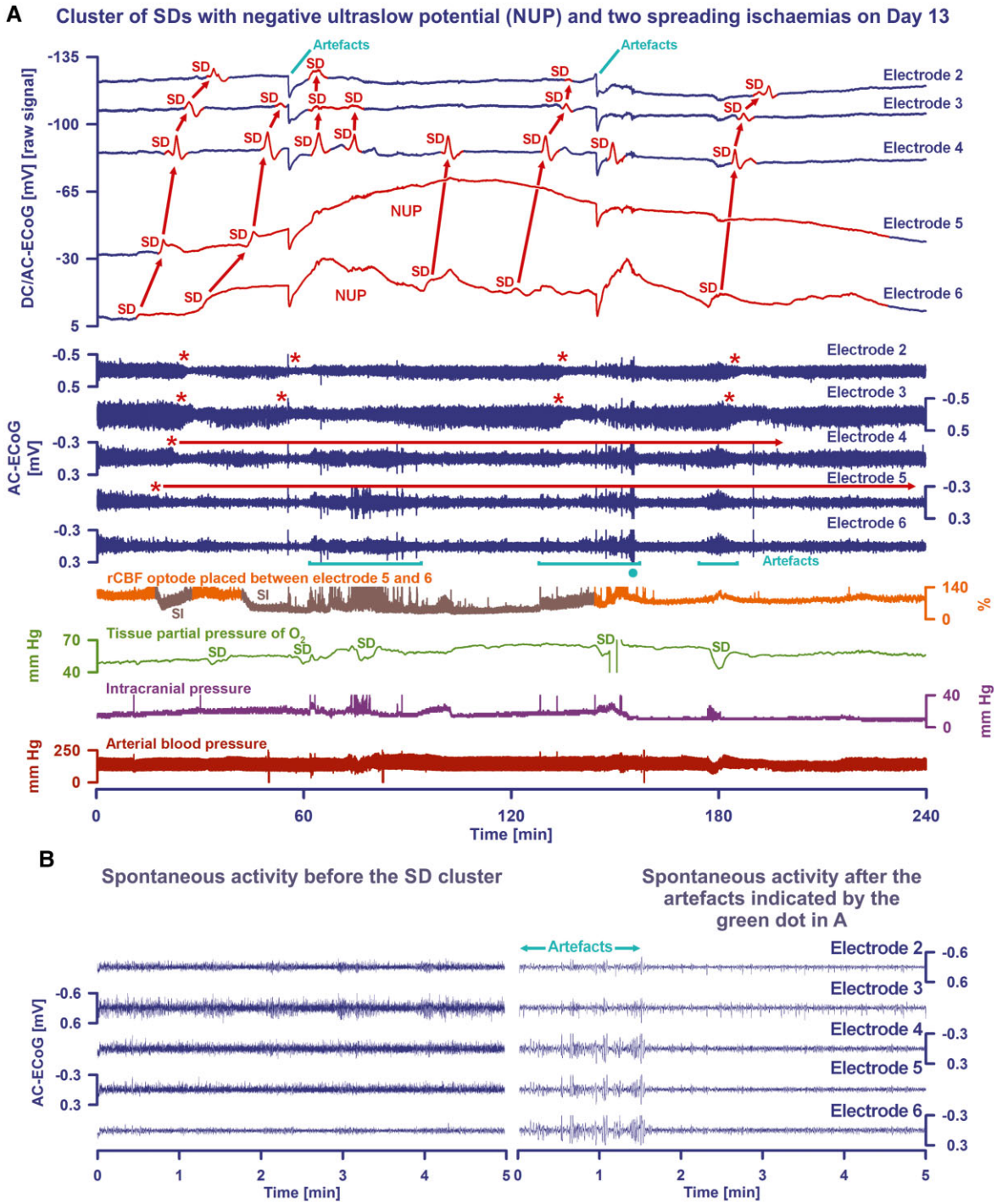

Figure 5 Example case of delayed infarction—second part. Example case of an SD cluster initiating a NUP, the electrophysiological correlate of infarction in human cerebral cortex.[4,6,8,11] (**A**) As illustrated in Fig. 4A, the patient developed a new delayed cortical infarct at electrodes 5 and 6 between two serial MRI scans on Days 8 and 15, and showed SDs indicating progressive disturbance of the neurovascular unit before Day 13. (**A**) The SD cluster on Day 13 that initiated the NUP at electrodes 5 and 6 and was accompanied first by a shorter- and then by a long-lasting spreading ischaemia (SI)[11,55] at the optode between electrodes 5 and 6 (marked in grey). Traces 1–5 from *top* to *bottom*: raw DC/AC-ECoG recordings (band-pass: 0–45 Hz). The first SD of the cluster started at electrode 6 and propagated to the other electrodes (first oblique arrow). At electrodes 6 and 5, which are located at the newly developing infarct, the SD changed into a NUP, to which further SDs were superimposed. At electrode 4, neighbouring the NUP-displaying electrode 5, SDs were particularly frequent. Not all of these SDs propagated to electrodes 3 and 2 (oblique arrows). Traces 6–10 show the depressive effect of the SDs on spontaneous activity (frequency band: 0.5–45 Hz). Since the beginning of the cluster there was practically no spontaneous activity at electrode 6. At the other electrodes, the first SD of the cluster induced a spreading depression of activity (red asterisks). At electrode 5, the activity depression was persistent, meaning that the activity did not recover (horizontal red arrow). Accordingly, the SDs were rated as isoelectric SDs and the patient showed a very long PTDDD (Fig. 4B).[26] At electrode 4, the first SD also led to a long-lasting depression of spontaneous activity, but the activity eventually recovered (horizontal red arrow). Trace 11 gives regional cerebral blood flow (rCBF) recorded with an optode between electrodes 5 and 6 (Fig. 4C).

(Continued)

multiple linear regression analysis. This was done separately for early and delayed parenchyma damage and for the combination of both on the basis of the manual segmentation of MRI and CT scans. In an additional analysis, ABT% of the same MRIs was chosen as the dependent variable.

In the prognostic part, three outcomes were considered: eGOS at 7 months, early death and delayed death until 7 months after the initial haemorrhage. In the first analysis, after careful inspection of the distribution of this variable and residuals in the corresponding analyses, Pearson correlation and multiple linear models were chosen to assess the prognostic impact of potential predictors. The analysis was split into four steps. Following the logic of the clinical course, only variables from the beginning of the observation period [Rosen–Macdonald Score (RMS),[3] World Federation of Neurosurgical Societies score (WFNS) and modified Fisher score (MFS)[32,33]] were included in the first step. In the second step, these variables were combined with all variables obtained during the early period of Days 0–3. In the third step, these variables were combined with all variables until the end of neuromonitoring. All variables, especially ICH + ECI + DCI damage and $ABT\%_{Day14}$, were included in the fourth step to obtain a final prognostic model. Patients with early death were excluded from steps three and four. Note that statistical methods for the prognosis of eGOS were identical to those in the association analyses for parenchymal damage volumes, but now the independent variables of the respective linear models were temporal predictors and not only associated factors.

The outcome early death was defined as death before the first follow-up image that allowed the assessment of parenchymal damage due to DCI. The outcome delayed death to follow-up was defined by categorizing the eGOS at 7 months (1 versus >1). Patients with early death were excluded from the analysis of delayed death. For both early and delayed death logistic regression analysis and ROC analysis were applied.

Standardized betas for the separate variables and *r*-square values of the entire model are presented for each linear multiple regression model. For multiple logistic regression models, odds ratios are presented. An analysis of residuals for linear models is included in the Supplementary material. The level of significance was 0.05 (two-sided). No correction for multiplicity was done as explained in the legend of Supplementary Table 3. Primary analysis and analyses of the association and prognostic part were performed with SPSS for Windows (release 26) and exploratory analyses with SigmaPlot v.14.0.

Data availability

Electronic recording, processing and storage of the data were approved by the data protection officer of the Charité—Universitätsmedizin Berlin (data protection votes from 28 May 2008 and 5 May 2014). The datasets analysed during the current study are not publicly available because the patient's informed consent only permits the data analysis and publication by the investigators.

Results

Study population

Median age was 55 years (IQR: 47–63). Supplementary Table 1 provides demographic data. Figure 2A depicts the manually segmented volumes of focal damage due to ICH, ECI and DCI in the whole brain and Fig. 2B in the hemisphere ipsilateral to the recording strip. Volumes did not differ significantly among these three most prominent aetiologies of focal brain damage after aSAH. The figures also report the numbers of patients affected. Semi-automatically segmented $ABT\%_{Day14}$ was significantly larger than $ABT\%_{early}$, confirming the relevant development of delayed focal damage ipsilateral to the recording strip during the first 2 weeks (Fig. 2C). Manually segmented ICH + ECI + DCI damage and semi-automatically segmented $ABT\%_{Day14}$ correlated strongly with each other, although $ABT\%_{Day14}$ included not only irreversibly damaged tissue but also vasogenic oedema (Fig. 3A). Overall, 6777 SDs in 161/180 (89.4%) patients and 238 electrographic seizures in 14/180 (7.8%) patients occurred during 234.4 weeks (4.5 years) of cumulative recording time. Supplementary Fig. 3 shows the daily determined SD variables from Days 0 to 14 after the initial haemorrhage. Supplementary Fig. 4 shows time courses of relevant monitoring variables, including intracranial pressure (ICP), mean arterial pressure (MAP), cerebral perfusion pressure, TCD-determined mean blood flow velocities (mbfv) of the ipsilateral MCA and Glasgow Coma Score (GCS). In addition, the distributions of PTDDD, $peak_{SD}$, $peak_{isoSD}$, $peak_{clusSD}$ and DNDs as well as daily cumulative doses of propofol and midazolam are given. Figures 4 and 5 illustrate an example case of delayed infarction.

Primary analysis

Ten patients died early. Ninety of 170 (52.9%) patients developed delayed infarction ipsilateral to the recording strip. In the primary analysis, we investigated whether a 60-min cut-off for $PTDDD_{delayed}$ (Fig. 4B) indicates delayed ipsilateral infarction with

Figure 5 Continued
The first SD induced a spreading ischaemia that lasted for 12 min and the second one a spreading ischaemia that lasted for about 90 min. During the second spreading ischaemia, rCBF fell to a level of 35% compared to the rCBF level before the cluster (=100%). Trace 12: brain tissue partial pressure of oxygen ($p_{ti}O_2$) recorded with a sensor in cerebral cortex in relative proximity to electrode 3. In this example, the oxygen probe was positioned outside the ischaemic zone. Thus, $p_{ti}O_2$ displayed a baseline value of about 50 mmHg before the SD cluster, which is above the normal range. While the SD-induced spreading ischaemias occurred at a distance of 2–3 cm, $p_{ti}O_2$ slowly continued to rise by about 15 mmHg, which was repeatedly interrupted for short times by SD-induced drops in $p_{ti}O_2$. SDs are often identified as steep drops in $p_{ti}O_2$ recordings, even if the haemodynamic responses are normal, because the cerebral metabolic rate of oxygen strongly increases during SD.[58] Trace 13: intracranial pressure. Trace 14: arterial blood pressure. Two large artefacts can be seen in the raw DC/AC recordings in **A**) (traces 1–5, marked in green). In addition, high-frequency artefacts occur in traces 6–10 and are particularly noticeable in traces 8–10 where there is hardly any spontaneous activity during the SD cluster. (**B**) The *left* part shows the spontaneous activity before the SD cluster at higher temporal resolution. The *right* part gives the spontaneous activity during the SD cluster during and after the artefact-laden time period indicated by the green circle in **A**. In the portion following the artefacts, it is visible that hardly any spontaneous activity has recovered at electrodes 4–6. When determining the depression period artefacts should not be confused with spontaneous activity, otherwise the duration of the depression period will be underestimated. Panel **B** thus illustrates that it is always necessary to consider not only post-processed signals but also the high-resolution original signals, although this increases the workload for the assessment.

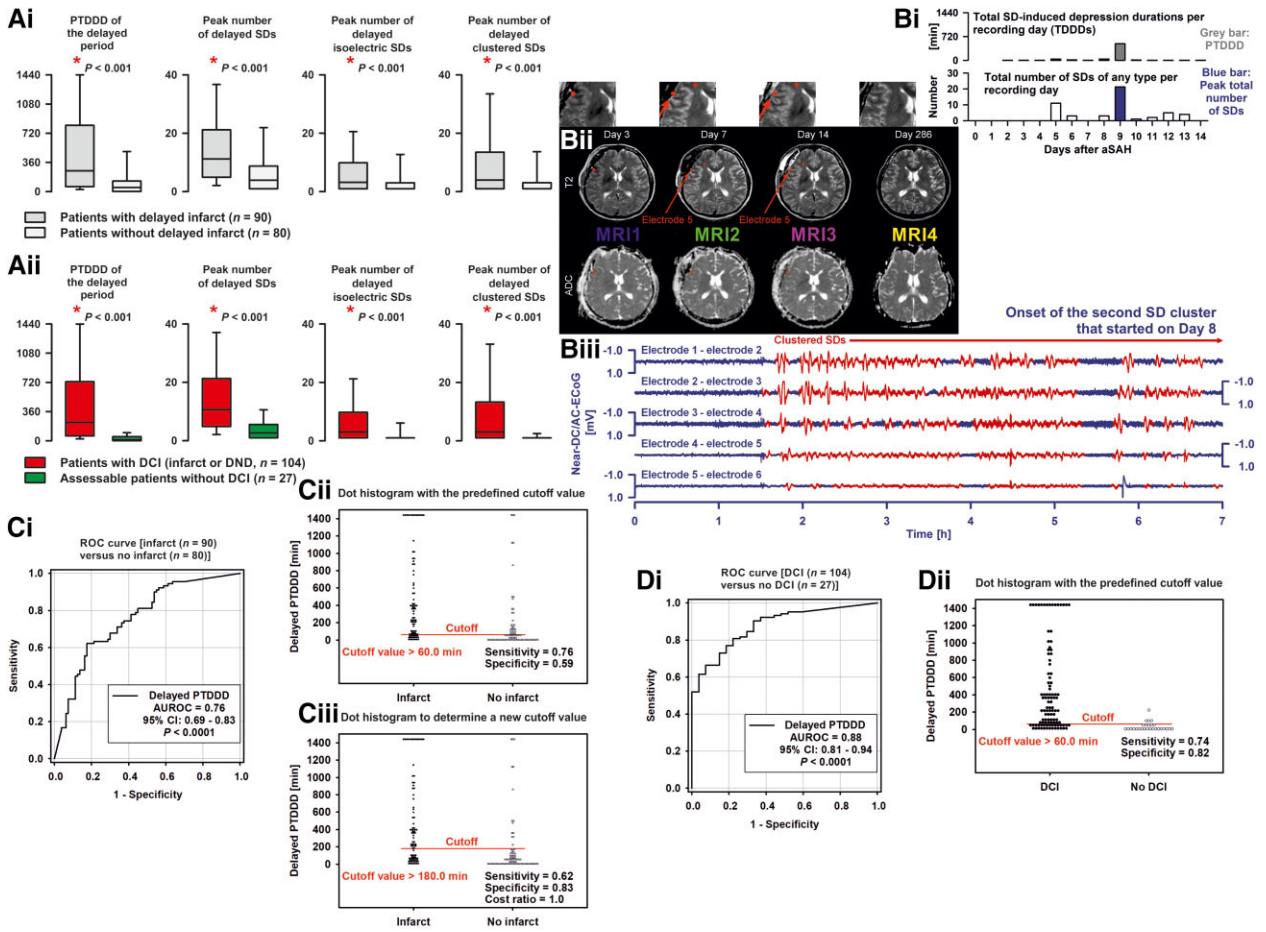

Figure 6 Delayed cerebral ischaemia—first part including primary analysis. (**A**) All four SD variables of the delayed period were significantly different between patients with and without delayed ipsilateral infarction [**A(i)**] or between patients with and without delayed cerebral ischaemia (DCI: delayed ipsilateral infarction and/or DND) [**A(ii)**] Mann–Whitney rank sum tests (MWRST)]. PTDDD = peak TDDD of a recording day during the delayed period ($PTDDD_{delayed}$). (**B**) Example case showing two SD clusters associated with reversible vasogenic cortical oedema but not infarction. In **B(i)**, SDs were counted and depression durations were scored for each day to determine the TDDD (*top* plot), and the total number of SDs per recording day (*bottom* plot). The PTDDD and peak SDs/day ($peak_{SD}$) were defined as the maximal values among all recording days (indicated with a dark grey and dark blue bar, respectively). The patient showed two SD clusters. The first one started on Day 5 and consisted of 14 SDs within 19 h. The second cluster started on Day 8 and included 34 SDs that occurred with decreasing frequency over the course of several days. In **B(ii)**, representative T_2-weighted (T2w) images and ADC maps are presented on the level of the basal ganglia with a slice thickness of 5 mm. No abnormal findings were detectable on the first post-operative MRI on Day 3 (MRI1). In contrast, T_2 imaging on Day 7 demonstrated increased signal intensity in the right insular cortex (red asterisk) adjacent to electrode 5 (red point) (MRI2). The hyperintense T_2 signal peaked on Day 14 (MRI3) (*inset*), whereas the follow-up MRI on Day 286 (MRI4) showed complete resolution of the abnormal T_2 signal. An ADC decrease was not noticeable at any time. This constellation suggests a reversible, vasogenic oedema of right insular cortex. Bipolar near-DC/AC-ECoG recordings were available in this patient.[26] In **B(iii)**, the beginning of the second SD cluster on Day 8 is displayed (SDs are marked in red). Of note in the clinical course was a reversible delayed neurological deficit with hemihypaesthesia of the left forearm and leg. The case illustrates that SD clusters were not always associated with new brain infarcts. Interestingly, very similar reversible vasogenic cortical accentuated oedema on MRI is also typically seen in severe cases of familial hemiplegic migraine, a rare Mendelian model of disease for SD and SD-induced spreading depression of activity.[45–47] (**C**) In the primary analysis (https://doi.org/10.1186/ISRCTN05667702), we investigated whether a 60-min cut-off for $PTDDD_{delayed}$ indicates delayed ipsilateral infarction with a sensitivity >0.60 and a specificity >0.80. [**C(i)**] The AUROC for $PTDDD_{delayed}$ to indicate delayed ischaemic stroke ipsilateral to the recording strip was 0.76 (95% CI: 0.69–0.83) and highly significantly larger than 0.5. [**C(ii)**] The primary analysis of the predefined 60-min cut-off was significant regarding sensitivity [= 0.76 (0.65–0.84), $P = 0.0014$] but failed regarding specificity [= 0.59 (0.47–0.70)] because the specificity was significantly lower than 0.80 ($P < 0.0001$). This means that the study failed to meet the primary end point. [**C(iii)**] However, we had also decided *a priori* that we would determine a new cut-off value if necessary (https://doi.org/10.1186/ISRCTN05667702). Based on a cost ratio of 1.0, a longer 180.0-min cut-off indicated delayed infarction with a sensitivity of 0.62 and a specificity of 0.83. [**D(i)**] In another predefined secondary analysis (https://doi.org/10.1186/ISRCTN05667702), we found that the performance of $PTDDD_{delayed}$ to indicate DCI (delayed ipsilateral infarction and/or DND) was higher than the performance of $PTDDD_{delayed}$ to indicate delayed infarction. [**D(ii)**] The predefined 60-min cut-off for $PTDDD_{delayed}$ indicated DCI with a sensitivity of 0.74 (0.65–0.82) and a specificity of 0.82 (0.62–0.94). However, this is reported with the caveat that (i) no sample size calculation was performed for the composite end point DCI (delayed ipsilateral infarction and/or DND); and (ii) there was a relatively large group of unconscious patients without delayed infarction for whom no clinical assessment was possible whether they had a reversible DND or not and for whom it therefore remained unclear whether they belonged to the DCI group or not. Accordingly, these patients had to be excluded from the analysis of the composite end point DCI.

a sensitivity >0.60 and a specificity >0.80. The primary analysis was significant regarding sensitivity {=0.76 [68/90, 95% confidence interval (CI): 0.65–0.84], $P = 0.0014$} but specificity was 0.59 (47/80, 0.47–0.70), i.e. significantly lower than 0.80 ($P < 0.0001$) [Fig. 6C(ii)]. However, the positive predictive value of the 60-min cut-off was 0.67 (68/101, 0.57–0.76), the negative predictive value was 0.68 (47/69, 0.56–0.79) and the AU ROC was 0.76 (CI: 0.69–0.83, $P < 0.0001$) [Fig. 6C(i)]. Therefore, we performed further analyses to better classify the result and, if possible, generate new hypotheses. As specified in 2008, we first performed a secondary analysis to determine a new cut-off for $PTDDD_{delayed}$. On the basis of a cost ratio of 1.0 (i.e. equal loss for false-positive or false-negative results), a longer 180.0-min cut-off indicated delayed infarction with a sensitivity of 0.62 and a specificity of 0.83 [Fig. 6C(iii)].

Prediction of DCI versus prediction of delayed infarction

When we considered only patients who either developed a delayed infarct ipsilateral to the recording strip or were sufficiently assessable clinically to determine whether they developed a reversible DND, the AUROC of $PTDDD_{delayed}$ to indicate DCI (reversible DND or ipsilateral infarction) was 0.88 (CI: 0.81–0.94, $P < 0.0001$) [Fig. 6D(i)]. Thus, $PTDDD_{delayed}$ was a stronger predictor for the composite outcome 'DCI' than for the primary outcome 'delayed infarction'. The predefined 60-min cut-off for $PTDDD_{delayed}$ indicated DCI with a sensitivity of 0.74 (0.65–0.82) and a specificity of 0.82 (0.62–0.94) [Fig. 6D(ii)].

Contrary to what we defined *a priori* in 2008 before the DISCHARGE-1 trial, it could be argued that the relative costs of a false-negative finding, i.e. overlooking the development of a delayed infarction, for therapeutic interventions with a good safety profile are much greater than those of a false-positive finding, i.e. treating a patient who does not develop a delayed infarction. It is also important that successful treatment is more likely if treatment is started earlier, following the motto 'time is brain'.[34] On this basis, it might be debated that a cost ratio of 0.7 is more appropriate than a cost ratio of 1.0. With a cost ratio of 0.7, we found a cut-off of 21.1 min for $PTDDD_{delayed}$ to indicate delayed ipsilateral infarction (sensitivity: 0.92, specificity: 0.44) and a cut-off of 23.7 min to indicate DCI (sensitivity: 0.90, specificity: 0.67).

Overall, all four SD variables of the delayed period were highly significantly different between patients with and without delayed infarction [Fig. 6A(i)] or between patients with and without DCI [Fig. 6A(ii)]. However, $PTDDD_{delayed}$ almost always performed better than the other variables, as shown in the multivariate analysis that follows (Supplementary Table 2).

Impaired consciousness and DCI

Figure 2H and I illustrate the importance of impaired consciousness, particularly in those aSAH patients who were at high risk for delayed infarction. The top graph in Fig. 2I shows that only 80/170 (47.1%) patients were clinically assessable during the delayed period. In non-assessable patients, median GCS was 3 (IQR: 3–3). In the remaining patients, GCS reached a value of 6, at least at times, so that the occurrence or absence of a DND-defining drop in GCS or new focal neurological impairment could be evaluated within certain limits (Supplementary material for the exact definition of DND). Overall, patients with delayed infarction showed a significantly lower median GCS than patients without delayed infarction (Fig. 2H). The bottom graph in Fig. 2I illustrates that within the group of delayed infarction patients, clinically non-assessable patients had significantly greater delayed infarct volume than clinically assessable patients. Figure 2J demonstrates that clinically assessable patients with delayed infarction were more likely to have a DND than patients without delayed infarction. However, DNDs were reversible in about one-third of cases, which in clinical parlance would be called a transitory ischaemic attack. On the basis of these results, we divided the patients into five groups for further exploratory analyses. In Fig. 2K–M, SD variables are compared between these five groups.

Characterization of reversible and permanent DNDs

In 40/43 (93.0%) patients, the diagnosis of a DND was based on a decrease on the GCS that could not be attributed to other causes and in 8/43 (18.6%) patients on new focal neurological impairment (such as hemiparesis or aphasia).[7] DND occurred at a median of Day 7 (IQR: 5–10) (Supplementary Fig. 4I). Typically, the DND-defining secondary drop in GCS [Fig. 3C(vi)] coincided with the peak of SDs, which began to increase in frequency and severity 1 to 2 days earlier [Fig. 3C(i–iv)]. TDDD and number of SDs per recording day were significantly higher on the day of DND than 3 days earlier [Fig. 3C(i and ii)]. The treating physicians typically responded to the clinical deterioration by increasing the doses of norepinephrine to induce hypertension [Fig. 3C(viii)]. Accordingly, we observed a significant increase in MAP in the days after the onset of DND [Fig. 3C(vii)]. TCD-determined mbfvs of the ipsilateral MCA to assess proximal vasospasm did not reach their maximum until 2 days after the onset of DND [Fig. 3C(v)]. Figure 6B shows an example of a reversible DND associated with a prominent SD cluster that was followed by vasogenic cortical oedema but not infarction.

Importantly, in clinically assessable patients that did not develop delayed infarction, the AUROC of $PTDDD_{delayed}$ to indicate a reversible DND was 0.84 (CI: 0.70–0.97, $P = 0.001$). The prespecified 60-min cut-off showed a sensitivity of 0.71 (0.42–0.92), a specificity of 0.82 (0.62–0.94), a positive predictive value of 0.67 (0.38–0.88) and a negative predictive value of 0.85 (0.65–0.96).

The infarct ratios among clinically non-assessable and assessable patients were 51/90 and 39/80, respectively, and thus 1.16 times higher in non-assessable patients. On the basis of the rate of reversible DNDs in assessable patients and the assumption that the incidence of reversible DNDs in non-assessable patients is similarly increased to the incidence of infarcts, it is estimated that 15/39 non-assessable patients without delayed infarction developed reversible DNDs. Within assessable patients without delayed infarction, the proportion of patients with $PTDDD_{delayed}$ above the 60-min cut-off was 15/41 (0.37). On the basis of this proportion and the correction factor of 1.16, it is estimated that $PTDDD_{delayed}$ should have been above the 60-min cut-off in $0.37 \times 1.16 \times 39 = 17$ non-assessable patients without delayed infarction. We found that $PTDDD_{delayed}$ was above the 60-min cut-off in 18/39 patients, which is very close to 17/39. The hypothesis that coma only masks, but does not protect against, the occurrence of reversible DNDs when the propensity for ischaemic infarcts actually increases is based on clinical plausibility. The two facts that (i) $PTDDD_{delayed}$ was significantly associated with the occurrence of reversible DNDs in assessable patients; and that (ii) the rate of patients with $PTDDD_{delayed}$ above the 60-min cut-off in non-assessable patients without delayed infarction was exactly in the expected range are not yet proof, but make it plausible that the association between reversible DNDs

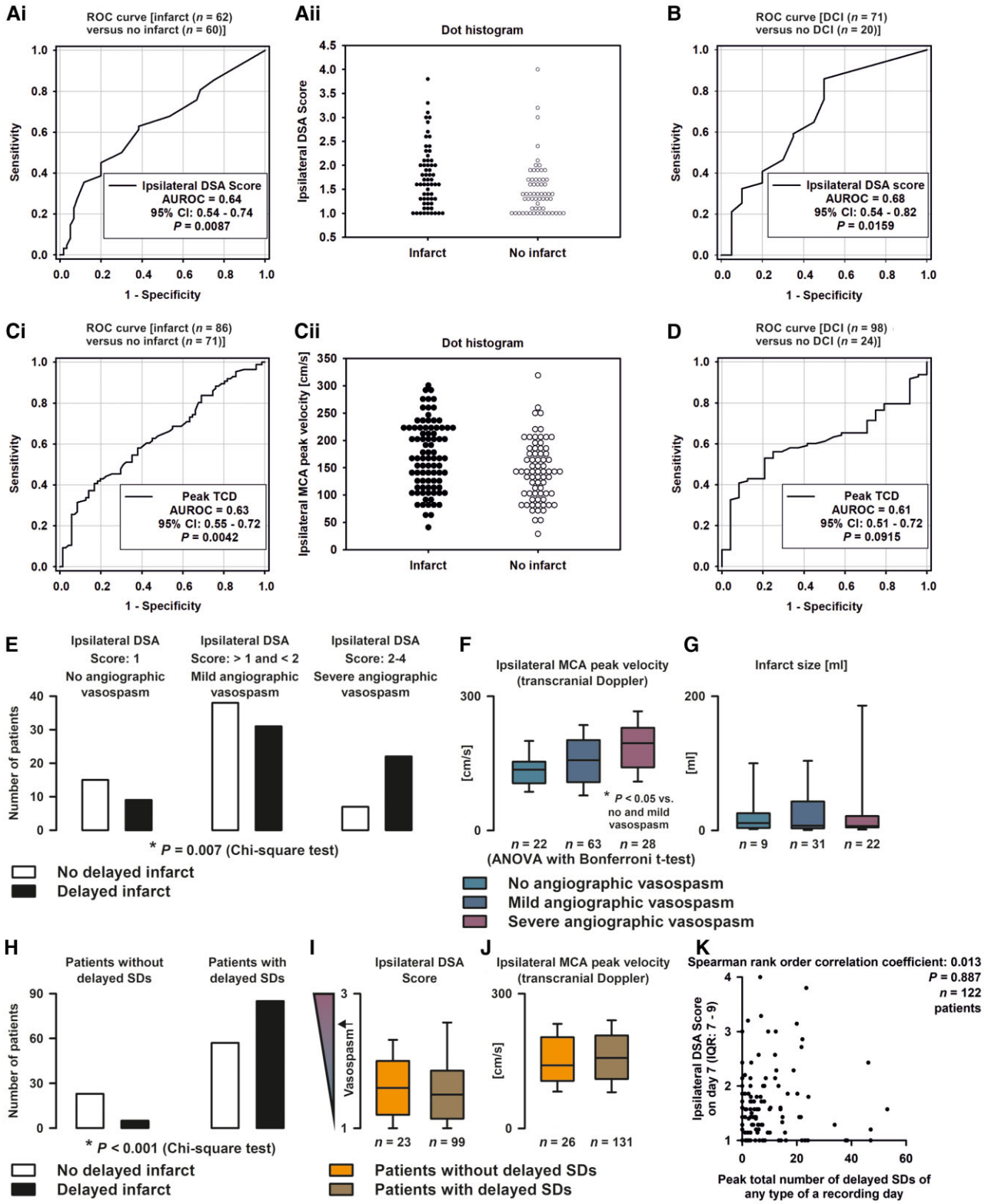

Figure 7 Delayed cerebral ischaemia—second part. The AUROC for the ipsilateral DSAS of the DSA around Day 7 to indicate delayed infarction ipsilateral to the recording strip (**A**) and DCI (**B**) were statistically significant (CI = confidence interval). In addition, the AUROCs for the highest TCD-determined mean blood flow velocity (mbfv) of the ipsilateral MCA to indicate delayed stroke ipsilateral to the recording strip (**C**) and DCI (**D**) were statistically significant. The AUROCs corresponded well with previous reports.[35,65] As pointed out previously in this context, a statistically significant association does not necessarily imply clinical utility as a diagnostic test.[35] A C-statistic value of 0.50 indicates no better predictive value than chance; a value of 0.60 is thought to be indicative of a diagnostic test with limited predictive value.[66] (**E**) Delayed infarcts also occurred in patients without angiographic vasospasm[67–71] and the absolute largest group of patients with most delayed infarcts had rather mild proximal vasospasm.

(Continued)

and $PTDDD_{delayed}$ exists not only for assessable but also for non-assessable, comatose patients.

Proximal vasospasm and DCI

DSA was performed on Day 7 (IQR: 7–9) to assess the occurrence of angiographic vasospasm ($n = 123$). Basal cerebral arteries ipsilateral to the recording strip could be assessed in 122 cases. As explained in Fig. 7E, DSAS of 1 meant no angiographic vasospasm, DSAS between 1 and 2 mild vasospasm and DSAS between 2 and 4 severe vasospasm. The AUROC was 0.64 (0.54–0.74, $P = 0.0087$) for the ipsilateral DSAS to indicate delayed infarction ipsilateral to the recording strip (Fig. 7A) and 0.66 (0.56–0.75, $P = 0.0026$) for the overall DSAS to indicate delayed infarction anywhere in the brain. TCD was performed once daily to measure mbfvs of the MCAs ($n = 163$).[35,36] In 157 cases, mbfvs of the MCA ipsilateral to the recording strip were available (Supplementary Fig. 4D). Similar to the DSAS, the highest mbfv of the ipsilateral MCA ($peak_{mbfv}$) showed an AUROC of 0.63 (0.55–0.72, $P = 0.0042$) for delayed infarction ipsilateral to the recording strip (Fig. 7C). The highest mbfv of both MCAs showed an AUROC of 0.65 (0.56–0.73, $P = 0.0016$) for delayed infarction anywhere in the brain. AUROCs of DSAS and $peak_{mbfv}$ for DCI were in a similar range as AUROCs for delayed infarction alone (Fig. 7B and D). Although delayed infarcts also occurred in patients without angiographic vasospasm, higher DSAS was associated with more delayed infarcts (Fig. 7E). Patients with higher DSAS showed higher $peak_{mbfv}$ (Fig. 7F). Delayed infarct sizes were not different between patients with and without angiographic vasospasm (Fig. 7G). Figure 7H–J illustrates that neither DSAS nor $peak_{mbfv}$ differed between patients with and without delayed SDs, although patients with delayed SDs were significantly more likely to develop delayed infarction than patients without delayed SDs. Neither DSAS nor $peak_{mbfv}$ correlated with any of the SD variables (Fig. 7K).

Association analysis with damage volumes

Figure 3D illustrates that $PTDDD_{entire}$ correlated positively with both ICH + ECI + DCI damage and $ABT\%_{Day14}$, and negatively with spatial distance between recording electrode and nearest lesion. Supplementary Fig. 5 provides an overview of correlations for standard and SD variables with manually segmented ICH + ECI damage and DCI damage.

Association analyses were performed for manually segmented (i) ICH + ECI damage; (ii) DCI damage; and (iii) ICH + ECI + DCI damage, including Pearson correlation analysis of each variable (Supplementary Table 3) followed by multiple linear regression.

In multiple regression models, ICH + ECI damage was associated with $PTDDD_{early}$ ($\beta = 0.450$, $P < 0.001$), RMS ($\beta = 0.214$, $P = 0.004$) and median GCS of the early period (GCS_{early}, $\beta = -0.157$, $P = 0.037$). The model explained 35% of variance in ICH + ECI damage (adjusted r-square). DCI damage was associated with $PTDDD_{delayed}$ ($\beta = 0.474$, $P < 0.001$), median $GCS_{delayed}$ ($\beta = -0.201$, $P = 0.005$) and $peak_{mbfv}$ ($\beta = 0.169$, $P = 0.016$). The model explained 35% of variance in DCI damage. ICH + ECI + DCI damage correlated with $PTDDD_{entire}$ ($\beta = 0.477$, $P < 0.001$), median GCS_{entire} ($\beta = -0.312$, $P < 0.001$) and RMS ($\beta = 0.176$, $P = 0.011$). Forty-four per cent of variance in ICH + ECI + DCI damage was explained by the prognostic variables. In simple regression, $PTDDD_{entire}$ alone explained 33% of variance in ICH + ECI + DCI damage.

In an alternative approach, we also performed association analyses for semi-automatically segmented $ABT\%_{early}$ and $ABT\%_{Day14}$ (see Supplementary Table 3 for Pearson correlation analyses). In multiple regression models, $ABT\%_{early}$ was associated with $peak_{clusSD}$ ($\beta = 0.351$, $P < 0.001$) and median GCS ($\beta = -0.230$, $P = 0.008$) of the early period. The model explained 19% of variance in $ABT\%_{early}$ (adjusted r-square). $ABT\%_{Day14}$ was associated with $PTDDD_{entire}$ ($\beta = 0.413$, $P < 0.001$) and median GCS_{entire} ($\beta = -0.306$, $P < 0.001$). This model explained 34% of variance in $ABT\%_{Day14}$. In simple regression, $PTDDD_{entire}$ alone explained 26% of variance in $ABT\%_{Day14}$. Thus, correlation of SD variables and median GCS with parenchymal damage based on semi-automatically segmented MRIs was not substantially different from their correlation with parenchymal damage based on manually segmented MRIs and CTs.

Outcome and mortality

Exploratory analysis revealed that patients with at least one SD showed ipsilateral focal damage more often than patients without SD (Fig. 2G), had larger ICH + ECI + DCI damage (Fig. 2D), larger $ABT\%_{Day14}$ (Fig. 2E) and worse eGOS [evaluated at 199 days (IQR: 100–308) = 7 months, Fig. 2F], resulting in a 3.1-fold increased relative risk (CI: 2.1–4.1) and a 42% increased absolute risk of poor outcome (eGOS 1–5 versus 6–8). Patient outcome at 7 months correlated negatively with ICH + ECI + DCI damage, $ABT\%_{Day14}$, $PTDDD_{entire}$ and RMS (Fig. 3B).

The statistical analysis of early and delayed death is presented next. Eight patients died while the ECoG was being recorded. Four out of eight showed progression to clinical brain death prior to circulatory collapse. All four developed a terminal SD cluster that transitioned to NUP. In two cases, one of which is shown in Fig. 8A, the terminal SD cluster preceded a crisis of ICP. Case three resulted from brainstem compression, and case four without massive ICP increase was previously published.[37] The other four patients died during abrupt hypoxia–ischaemia after withdrawal of life-sustaining treatments, showing characteristic terminal SD. Three of these cases were previously published as part of a series which also included six patients dying from complications

Figure 7 Continued
(**F**) Panel confirms that higher $peak_{mbfv}$ was associated with more severe angiographic vasospasm. (**G**) Panel shows that ipsilateral delayed infarct sizes did not differ between patients with severe, with mild or without ipsilateral angiographic vasospasm. The definition of severe, mild and no angiographic vasospasm in **F** and **G** was based on the DSAS, as explained in **E**. (**H**) Delayed infarcts were more likely in patients with delayed SDs than in patients without delayed SDs. (**I**) The DSAS was similar between patients with and without delayed SDs. (**J**) The $peak_{mbfv}$ was similar between patients with and without delayed SDs. (**K**) A scatter plot demonstrating the lack of correlation between DSAS and peak total number of delayed SDs of a recording day ($peak_{SD}$). Thus, restricted upstream blood supply due to proximal vasospasm seems to have a modulating influence, but the statistical results challenge the concept that it is predominantly responsible for the development of delayed infarction. These findings complement previous observations that proximal vasospasm can be robustly antagonized without resounding success in prophylaxis of DCI.[72,73] Furthermore, similar to the present study, no clear association between proximal vasospasm and patient outcome was previously found,[65] in contrast to the clear association between DCI and poor outcome.[74] Overall, our results provide further evidence that the primary pathophysiological problem of delayed ischaemia is more distal to proximal vasospasm and involves the entire neurovascular unit.[10,11,55]

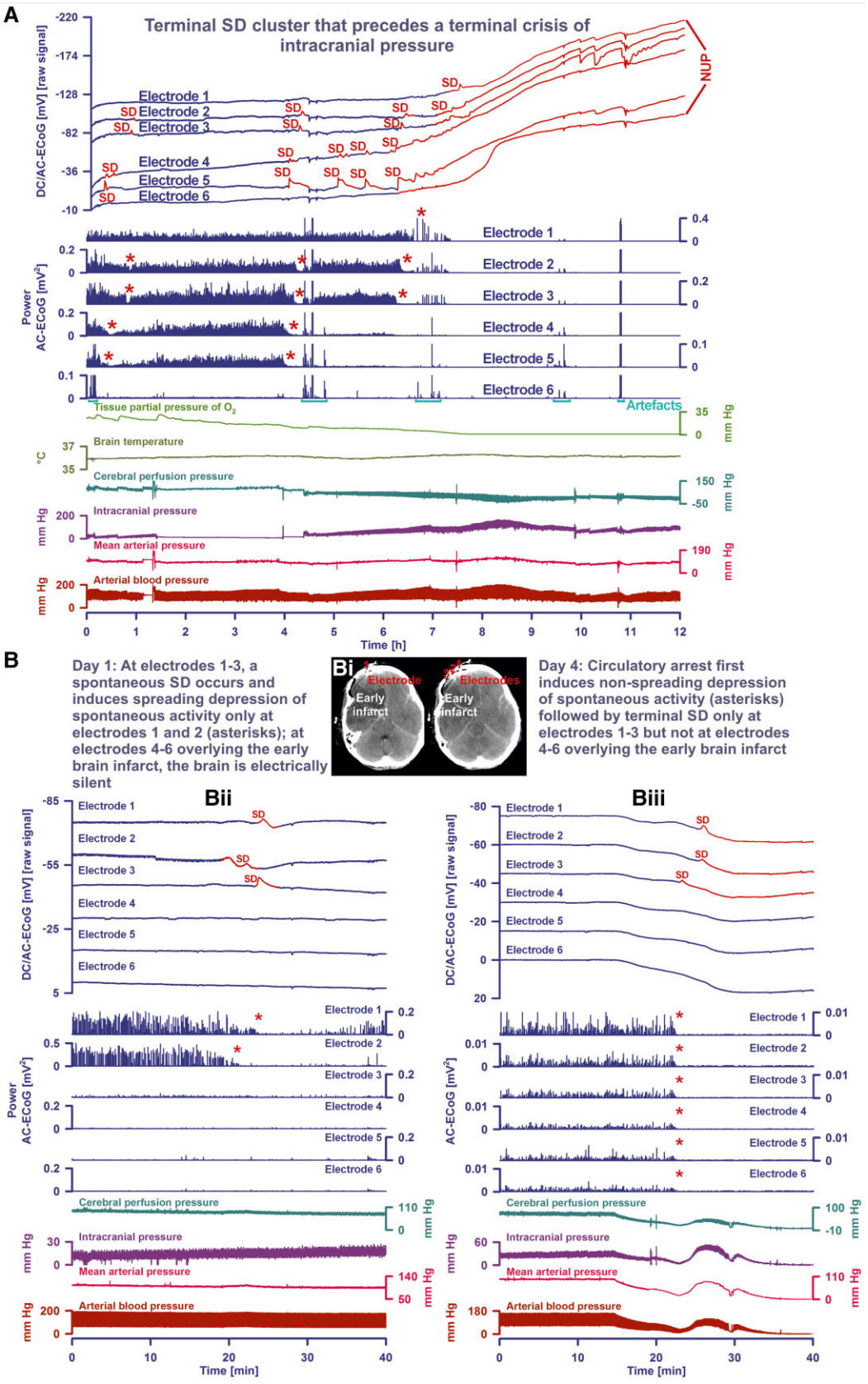

Figure 8 Brain death and death in the wake of circulatory arrest. (**A**) Terminal SD cluster that precedes a terminal crisis of ICP and progression to brain death. The patient suffered aSAH from rupture of an aneurysm of the right MCA. She initially showed a large intracerebral haematoma (ICH) of 43 ml and a malignant early infarct of 209 ml. However, the subdural electrode strip was placed over vital right frontal cortex. The terminal SD cluster

(Continued)

following either traumatic brain injury or malignant hemispheric stroke.[38] Another instructive case was discovered later during the analysis and is shown as an example in Fig. 8B.

Prognosis of eGOS at 7 months

Pearson analyses are presented in Supplementary Table 4.

(i) Among initial clinical scores, only RMS remained significant in multiple regression. This model explained 18% of eGOS variance (adjusted *r*-square).
(ii) Among initial clinical scores and monitoring variables of the early period, $PTDDD_{early}$ ($\beta = -0.442$, $P < 0.001$) and RMS ($\beta = -0.331$, $P < 0.001$) remained significant. This model explained 34% of eGOS variance.
(iii) Among initial clinical scores and monitoring variables of the entire period, $PTDDD_{entire}$ ($\beta = -0.271$, $P = 0.007$), $peak_{isoSD\text{-}entire}$ ($\beta = -0.212$, $P = 0.035$) and RMS ($\beta = -0.408$, $P < 0.001$) were significant prognostic factors in multiple regression. This model explained 36% of eGOS variance.
(iv) Among all variables including neuroimaging after the end of monitoring, ICH + ECI + DCI damage ($\beta = -0.284$, $P < 0.001$), RMS ($\beta = -0.302$, $P < 0.001$), $peak_{isoSD\text{-}entire}$ ($\beta = -0.271$, $P < 0.001$) and DCI-category ($\beta = -0.175$, $P = 0.013$) were included in the final model, explaining 45% of eGOS variance.

In simple regression, $PTDDD_{entire}$ alone explained 25% of overall eGOS variance ($n = 162$).

Prognosis of early death

Early death before the first neuroimage for the assessment of DCI occurred in 10 of 180 patients. Among initial clinical scores, the largest AUROC was found for RMS (0.69, CI: 0.56–0.82), followed by WFNS (0.68, 0.50–0.85). MFS was not predictive (0.53, 0.36–0.71). Among the SD variables, $PTDDD_{early}$ showed the largest AUROC (0.87, 0.79–0.95), followed by $peak_{isoSD\text{-}early}$ (0.73, 0.56–0.90), $peak_{SD\text{-}early}$ (0.64, 0.52–0.76) and $peak_{clusSD\text{-}early}$ (0.58, 0.43–0.73). Median MAP_{early} was not predictive (0.49, 0.35–0.62), whereas median ICP_{early} showed an AUROC of 0.73 (0.57–0.89). The largest AUROC of all variables was shown by ICH + ECI damage with AUROC 0.88 (0.75 to <1.0). None of the patients who died early had an MRI. Therefore, association between early death and $ABT\%_{early}$ could not be investigated. Multiple regression was not performed due to the small number of 10 events.

Prognosis of delayed death

All 10 patients who died prematurely were excluded from this analysis. Due to missing values, only 152 of the remaining 170 patients could be included. Thirty-two of 152 patients (21.1%) had passed away after 7 months. Among clinical scores at the beginning of the observation period, the largest AUROC was found for RMS (0.70, 0.61–0.80), followed by WFNS (0.64, 0.54–0.74). MFS was not predictive (0.57, 0.46–0.67). Early measurements of SD variables, GCS, MAP, ICP, ICH + ECI damage and $ABT\%_{early}$ were inferior to measurements over the entire neuromonitoring period or at the end of this period and are not reported here. DSAS, $peak_{mbfv}$ and median MAP for the entire neuromonitoring period were not predictive (AUROC < 0.6). Among SD variables of the entire neuromonitoring period, $PTDDD_{entire}$ showed the largest AUROC (0.76, 0.67–0.85), followed by $peak_{isoSD\text{-}entire}$ (0.70, 0.60–0.81), $peak_{SD\text{-}entire}$ (0.70, 0.60–0.80) and $peak_{clusSD\text{-}entire}$ (0.68, 0.57–0.79). Median GCS_{entire} showed an AUROC of 0.67 (0.57–0.76) and median

Figure 8 Continued
started on Day 5 while the extraventricular drainage (EVD) catheter was left open to counteract an increase in ICP to 24 mmHg. The second SD led to a spreading depression of activity, which was reversible only at electrodes 1–3, while at electrode 5 a persistent activity depression developed. Recovery of the spontaneous activity at electrode 4 was also practically negligible. At the same time, brain tissue partial pressure of oxygen ($p_{ti}O_2$) showed a biphasic decrease, which might have resulted from disturbed autoregulation during the first phase, as it initially followed a decrease in mean arterial pressure (MAP),[75] and from SD during the second phase.[64,76] Twenty-five minutes after this first SD of the terminal cluster, the EVD was closed again. At this point, ICP was 32 mmHg. Two further SDs occurred at electrodes 4 and 5, not involving electrodes 1–3, while ICP further increased to 63 mmHg and cerebral perfusion pressure (CPP) and $p_{ti}O_2$ declined to 37 and 7.8 mmHg, respectively. At this point, the NUP-initiating SD started at electrode 4, spreading to electrodes 5 and 3, and induced spreading depression of activity at electrodes 1–4. The $p_{ti}O_2$ showed a further drop from 7.8 to 5.6 mmHg during this SD. This was most probably induced by the SD, as it did not follow ICP or MAP. While ICP continued to rise slowly to 120 mmHg over the next 2 h until it was as high as MAP, and CPP and $p_{ti}O_2$ dropped accordingly to zero, further SDs superimposed on the NUP occurred at different electrodes. Finally, the NUP only appeared as a smooth line. The median amplitude of the NUP at the six different electrodes was −160 mV, which is in the range of previous observations during the development of brain death.[37,48] The patient was found to have loss of brainstem reflexes and fixed dilated pupils. After discussion with the family regarding the poor prognosis, the patient was terminally extubated. The circulatory arrest occurred 11 h after her brain death. The SD-induced ICP increase is thought to be explained as follows. Along with SD-initiated cytotoxic oedema, increased tissue content of Na^+, Cl^- and water gradually develops in the wake of focal ischaemia.[12,77–80] This so-called ionic oedema can be life-threatening because it can increase ICP. Experimentally, CSF surrounding the brain has been identified as the source of ionic oedema by penetrating the tissue through perivascular flow channels.[14] This process was initiated by SDs along with SD-induced spreading ischaemia, which in turn enlarged perivascular spaces and doubled glymphatic inflow speeds. (**B**) Terminal SD in the wake of circulatory arrest. The patient suffered an aSAH from rupture of a right posterior communicating artery aneurysm. An MRI scan on Day 1 already showed a large early cerebral infarct of 164 ml. [**B(i)**] Two neighbouring slices of a CT study on Day 3 that revealed the increase of a midline shift from 10 to 14 mm compared to a CT of the previous day. Electrodes 1–3, marked by the red numbers '1', '2' and '3', were positioned over vital tissue. In contrast, electrodes 4-6 were located over the infarct (not shown). [**B(ii)**] Example of an early SD. These SDs were exclusively recorded by electrodes 1–3 overlying vital tissue, but not by electrodes 4–6 over the necrosis. Interestingly, the SD was not first seen at the electrode closest to the infarct, but at electrode 2, i.e. there was a reverse direction of SD propagation from the periphery towards the ischaemic centre, similar to late SDs in patients with malignant hemispheric stroke[81] and in animal models of focal ischaemia.[51,82] Electrode 3 did not display spontaneous activity. Accordingly, the SD met the criteria of an isoelectric SD.[26,30] At electrodes 1 and 2, the SD induced a spreading depression of spontaneous activity (marked by red asterisks). [**B(iii)**] On Day 4, ICP increased to 30 mmHg despite treatment with sufentanil, propofol, midazolam and mannitol and the patient's right pupil became increasingly dilated. At this point, the spontaneous brain activity was characterized by a burst-suppression pattern with tiny bursts decreasing in amplitude from electrodes 1–6. Eventually a Do Not Resuscitate–Comfort Care order was activated after family discussion and the patient was terminally extubated. Withdrawal of the life-sustaining treatment resulted in a drop of mean arterial pressure below 30 mmHg. At about the same time, the remaining spontaneous brain activity of very low amplitude completely disappeared demonstrating the typical pattern of a non-spreading depression of spontaneous activity (marked by red asterisks).[38] (**Biii**) The time course of the systemic arterial pressure including the circulatory arrest and subsequent terminal SD that started at electrode 3 23 s after complete cessation of the spontaneous brain activity. The terminal SD then spread from electrode 3 to electrodes 2 and 1. Electrodes 4–6 overlying the early infarct did not show a terminal SD. In contrast, large positive homogeneous DC drifts were seen at all electrodes. These homogeneous DC drifts are most probably due to interferences of pCO_2, pH and pO_2 with the subdural platinum-iridium electrodes.[37]

ICP_{entire} of 0.62 (0.51–0.74). Neuroimaging variables after neuromonitoring showed the largest AUROC (ICH + ECI + DCI damage: 0.77, 0.69–0.86, $ABT\%_{Day14}$: 0.84, 0.76–0.93).

Subsequently, we performed two multiple logistic regression analyses. In the first model, $ABT\%_{Day14}$ was used as the neuroimaging variable, i.e. the analysis was based only on MRIs ($n = 129$). In the second model, ICH + ECI + DCI damage was used as the neuroimaging variable, i.e. the analysis was based on both MRIs and CTs ($n = 152$). In the first multiple logistic regression model, $ABT\%_{Day14}$ [odds ratio (OR): 23.62, $P = 0.011$], $PTDDD_{entire}$ (OR: 3.85, $P = 0.047$) and RMS (OR: 1.67, $P = 0.005$]) were significant. The related AUROC was 0.90 (0.84–0.96, corrected via leaving one out: 0.87, 0.79–0.94). In the second model, $PTDDD_{entire}$ (OR: 12.04, $P < 0.001$), RMS (OR: 1.61, $P = 0.001$) and median ICP_{entire} (OR: 1.26, $P = 0.005$) were significant. The related AUROC was 0.87 (0.80–0.94, corrected via leaving one out: 0.89, 0.82–0.95). See Supplementary material and Supplementary Tables 2–13 for further details of the multivariate statistical analyses.

Finally, we also explored the question of whether risk stratification for the delayed phase is already possible in the early phase (Days 0–3). This analysis is further explained in the Supplementary material and Supplementary Tables 14–16. In brief, only $PTDDD_{early}$, but no other variable measured either initially or during the early phase (RMS, MFS, WFNS, ICH + ECI damage, $ABT\%_{early}$, other SD variables, median GCS, MAP or ICP) was an independent predictor for the composite end point 'early death or DCI' in multivariate analysis ($P = 0.0070$). However, the AUROC of this early marker was 0.63 (0.54–0.71), which is insufficient for individual prediction.

Finally, Supplementary Fig. 6A shows the decay of spontaneous brain activity from Days 0 to 14 after the initial haemorrhage. Supplementary Fig. 6B shows that the greater the focal brain damage and the worse the patient's overall outcome, the smaller the amplitudes of spontaneous brain activity were on the last day of recording.

Discussion

DISCHARGE-1 failed to meet the primary end point, as the sensitivity of 0.76 for the predefined 60-min cut-off was significant but the specificity of 0.59 was significantly worse than 0.80. Nevertheless, a significant association between $PTDDD_{delayed}$ and delayed infarction was confirmed. Predictive values were 0.67 (positive) and 0.68 (negative), the AUROC was 0.76 and highly significantly larger than 0.5 ($P < 0.0001$). With a 180-min cut-off the targeted sensitivity was 0.62 and the specificity 0.83. Overall, the results indicate that 'delayed infarction' as a primary end point was somewhat misleading, as patients with reversible DND were classified as uneventful on the basis of this end point. DCI, like any other form of cerebral ischaemia, always initially leads to a reversible phase of neuronal cytotoxic oedema that develops into infarction in only a subset of cases,[7] and SD is experimentally the electrophysiological correlate of this initial, still-reversible phase of neuronal cytotoxic oedema.[12–16] Accordingly, in clinically assessable patients not developing delayed infarction, the AUROC of $PTDDD_{delayed}$ to indicate a reversible DND was 0.84 and was significantly >0.5 ($P = 0.001$). Predictive values of the prespecified 60-min cut-off were 0.67 (positive) and 0.85 (negative) for a reversible DND. At the 60-min cut-off, it is therefore sufficiently clear that injury has just developed, but in contrast to the 180-min cut-off, it is not yet sufficiently clear whether the injury will spontaneously resolve or progress to infarction (= tissue necrosis).

It was previously visualized in animals by various combinations of electrophysiological and imaging modalities, including DWI–MRI, that SD and neuronal cytotoxic oedema represent two different modalities of the same event.[12–16,39,40] Continuous high-resolution MRI is technically feasible during neurocritical care but still far away in clinical practice. It is also currently not possible to cover the entire brain surface with electrodes in aSAH patients. With the current state of the art, we were able to image focal damage at an early and a late time point, and also determine SD variables through the delayed imaging time point based on ECoG monitoring along 5 cm of brain surface. Despite temporal and spatial sampling limitations of imaging and ECoG, respectively, we found that the SD variables were highly significant in all correlation analyses, and were included in each of the multiple regression models of early, delayed and total focal brain damage, patient outcome at 7 months and death, strongly supporting that they are an independent biomarker of progressive brain injury in all conditions and time windows studied. In simple regression, $PTDDD_{entire}$ alone explained 33% of manually segmented ICH + ECI + DCI-damage variance, 26% of $ABT\%_{Day14}$ variance and 25% of overall eGOS variance. Contributing factors to these results might be: (i) that neurosurgeons usually targeted the electrode strip to the vascular territory of the aneurysm-carrying vessel, as this is often covered with blood and thus a predilection site for DCI; (ii) that the strip was usually placed far enough away from lesions, as necrotic tissue no longer produces SDs; (iii) that regional ECoG monitoring allows remote detection of metabolically stressed zones, as SDs spread widely originating from these zones; and (iv) that the neurosurgeons recruited patients into invasive neuromonitoring when they assumed a high risk for DCI on the basis of WFNS and preinterventional CT.

Even detection of a single SD resulted in the patient having a 3-fold increased relative risk and 42% increased absolute risk of poor outcome. Again, it is important to caution, however, that these results do not suggest that SDs are always associated with lesion development and permanent clinical deterioration. Previous imaging studies on changes in regional cerebral blood flow or its surrogates suggested that SD is the pathophysiological correlate of migraine aura.[41–43] Accordingly, SD and SD-induced activity depression were recently recorded using ECoG in an aSAH patient while she had symptoms of migraine aura.[44] Figure 6 shows an example of how a pronounced SD cluster could occur and still not be followed by an infarct, but only by vasogenic cortical oedema.[45–47] Nonetheless, as previously observed,[4,6,11] SDs can transition to a NUP in a proportion of cases after aSAH, and subsequent neuroimaging then almost always showed a new infarct at the recording site.[8] In addition, whenever the dying process was recorded during our study, at least one SD marked the transition phase between life and death.[37,38,48] These findings, perhaps seemingly contradictory at first glance, can be plausibly explained by the fact that SDs during migraine aura, transitory ischaemic attack, stroke and dying occur along a complex continuum, as reviewed previously.[49,50] The present results strengthen this pathophysiological concept, not only via further examples but especially via the robust correlation between SD variables and the development of focal brain damage. Along this continuum, SDs can occur as a result of a mismatch between oxidative substrate supply and demand, but they can also be triggered by many noxious stimuli other than ischaemia.[51–53] Of particular relevance to the pathophysiology of aSAH is that SDs can be either the consequence or cause of severe vasoconstriction and ischaemia.[54,55] To further complicate matters, SDs have deleterious effects, such as the neuronal calcium surge and the increase

in energy demand due to intraneuronal sodium-induced sodium pump activation, but adaptive effects are also discussed.[11,52,56–60] Overall, in agreement with the original hypothesis based on the discovery of the inverse haemodynamic response to SD in animals, the results provide further evidence that it is especially the shift of the normal haemodynamic response towards the inverse haemodynamic response that disrupts the fragile equilibrium and causes the transition from SD to NUP, to continued cytotoxic oedema and to irreversible cellular damage.[55]

Of note, the rate of delayed infarcts was 90/170 (=53%) in DISCHARGE-1, much higher than the 20% rate assumed in the sample size calculation in 2008. Most probably, this resulted from the high severity of aSAH. A possible consequence of relatively high infarct frequencies is that cut-offs based on cost ratios are shifted towards higher sensitivities compared with the situation with moderate infarct frequencies. Recommendations derived from DISCHARGE-1 therefore relate primarily to high-risk aSAH populations.

In conclusion, our findings indicate that focal brain damage after aSAH is crucial for the patient's prognosis and not completed in the early phase but is decisively shaped by the late phase. We suggest that SDs can serve as a detector of reversible neurological deficits and impending infarcts, particularly in unconscious patients, to identify aSAH patients in real time who are most likely to benefit from targeted management strategies. We propose that a 25-min cut-off for $PTDDD_{delayed}$ is an appropriate first 'alert level' to review the patient's status and initiate tier 1 of targeted management strategies. We would make this recommendation although it is still relatively uncertain after 25 min whether the event will be reversible or progress to infarction. We suggest that tier 1 management adjusts targets for physiological interventions that are expected to modulate the development of SD. This includes careful assessment of basal variables such as MAP, ICP, cerebral perfusion pressure, respiration, body temperature and, if available, brain tissue partial pressure of oxygen. In addition, a blood gas analysis including measurement of glucose and electrolytes should be performed and it should be investigated whether inflammatory parameters are elevated or organ dysfunctions, especially of the kidneys or heart, or anaemia have occurred.

The very practical consequence for the intensivist is therefore to activate tier 1 at Minute 25 if, for example, an SD with a depression duration of 25 min occurs in a comatose patient, even though no SD occurred in the 23 h and 35 min beforehand. However, tier 1 should also be activated if two SDs have occurred within the last 24-h period, the first of which had a depression duration of 12 min and the second of which had a depression duration of 13 min, giving a total of 25 min. At Minute 25, tier 1 should be activated. If the cumulative SD-induced depression duration of the just-past 24-h period has then exceeded 180 min, the patient has developed a new infarct with 0.62 sensitivity and 0.83 specificity, implying that rescue therapy should not wait 180 min. We propose a 60-min cut-off as an appropriate moment to initiate rescue therapy because it indicates still-reversible DND with 0.71 sensitivity and 0.82 specificity. The type of rescue therapy is another highly controversial discussion.[61] The tenet espoused by Max Planck also applies to this discussion: 'Insight must precede application'. More research is therefore needed to understand the mechanisms underlying delayed ischaemia. In addition, neuromonitoring-guided management algorithms should be further optimized through feasibility studies.[26,62] At a later stage, they may be incorporated into interventional proof-of-concept trials.[63] Automated analysis techniques are under development and will be important in practice if real-time ECoG recordings are used to inform treatment decisions.[26]

Acknowledgements

We thank all the trial participants for their participation in the study and commitment to advancing knowledge regarding aSAH, and focal and global brain damage. We would like to thank the study nurses and the nursing staff of the participating intensive care units, without whose help this study would not have been possible. We appreciate the data and safety monitoring board. The paper is dedicated to Rudolf Graf, site investigator in Cologne and steering committee member, and to Christoph Drenckhahn, data manager in Berlin. Both inspired us with their enthusiasm for translational research, one as a senior, the other as a young scientist. Unfortunately, they did not live to see the publication of DISCHARGE-1 after all the work they did for it.

Funding

J.P.D., O.W.S., G.Bo., P.V., A.F., P.M. and J.W. report a grant from the Deutsche Forschungsgemeinschaft (German Research Council) (DFG DR 323/5-1). J.P.D. and A.F. report grants from the German-Israeli Foundation (GIF No. 124/2008), Era-Net Neuron 01EW1212 and Era-Net Neuron EBio2 with funds from BMBF 01EW2004 and CIHR Award No. NDD 168164. J.P.D. and O.W.S. report a grant from the EU 7th Framework Programme for Research (FP7): no 602150 CENTER-TBI. In addition, J.P.D. reports the following grants that supported secondary objectives of the study: DFG SFB Tr3 D10, DFG DR 323/6-1, DFG DR 323/10-1; Bundesministerium für Bildung und Forschung (German Federal Ministry of Education and Research) BMBF Centre for Stroke Research Berlin 01 EO 0801, BMBF Bernstein Centre for Computational Neuroscience 01GQ1001C B2 and BMBF NeuroCure SESAH EXC 257/2. NH is Berlin Institute of Health Clinical Fellow, funded by Stiftung Charité. M.S. reports support from the 'Friedrich C. Luft' Clinical Scientist Pilot Program funded by Volkswagen Foundation and Charité Foundation. J.W. reports the following grants: DFG WO 1704/1.1 and DFG WO 1704/1.2.

Competing interests

The authors report no competing interests.

Supplementary material

Supplementary material is available at *Brain* online.

References

1. Lawton MT, Vates GE. Subarachnoid hemorrhage. *N Engl J Med*. 2017;377:257–266.
2. Macdonald RL, Schweizer TA. Spontaneous subarachnoid haemorrhage. *Lancet*. 2017;389:655–666.
3. Rosen DS, Macdonald RL. Grading of subarachnoid hemorrhage: Modification of the World Federation of Neurosurgical Societies scale on the basis of data for a large series of patients. *Neurosurgery*. 2004;54:566–575; discussion 575–6.

4. Oliveira-Ferreira AI, Milakara D, Alam M, *et al*. Experimental and preliminary clinical evidence of an ischemic zone with prolonged negative DC shifts surrounded by a normally perfused tissue belt with persistent electrocorticographic depression. *J Cereb Blood Flow Metab*. 2010;30:1504–1519.
5. Eriksen N, Rostrup E, Fabricius M, *et al*. Early focal brain injury after subarachnoid hemorrhage correlates with spreading depolarizations. *Neurology*. 2019;92:e326–e341.
6. Hartings JA, York J, Carroll CP, *et al*. Subarachnoid blood acutely induces spreading depolarizations and early cortical infarction. *Brain*. 2017;140:2673–2690.
7. Vergouwen MD, Vermeulen M, van Gijn J, *et al*. Definition of delayed cerebral ischemia after aneurysmal subarachnoid hemorrhage as an outcome event in clinical trials and observational studies: Proposal of a multidisciplinary research group. *Stroke*. 2010;41:2391–2395.
8. Lückl J, Lemale CL, Kola V, *et al*. The negative ultraslow potential, electrophysiological correlate of infarction in the human cortex. *Brain*. 2018;141:1734–1752.
9. Macdonald RL, Higashida RT, Keller E, *et al*. Clazosentan, an endothelin receptor antagonist, in patients with aneurysmal subarachnoid haemorrhage undergoing surgical clipping: A randomised, double-blind, placebo-controlled phase 3 trial (CONSCIOUS-2). *Lancet Neurol*. 2011;10:618–625.
10. Pluta RM, Hansen-Schwartz J, Dreier J, *et al*. Cerebral vasospasm following subarachnoid hemorrhage: time for a new world of thought. *Neurol Res*. 2009;31:151–158.
11. Dreier JP. The role of spreading depression, spreading depolarization and spreading ischemia in neurological disease. *Nat Med*. 2011;17:439–447.
12. Dreier JP, Lemale CL, Kola V, Friedman A, Schoknecht K. Spreading depolarization is not an epiphenomenon but the principal mechanism of the cytotoxic edema in various gray matter structures of the brain during stroke. *Neuropharmacology*. 2018;134:189–207.
13. Murphy TH, Li P, Betts K, Liu R. Two-photon imaging of stroke onset in vivo reveals that NMDA-receptor independent ischemic depolarization is the major cause of rapid reversible damage to dendrites and spines. *J Neurosci*. 2008;28:1756–1772.
14. Mestre H, Du T, Sweeney AM, *et al*. Cerebrospinal fluid influx drives acute ischemic tissue swelling. *Science*. 2020;367:eaax7171.
15. Kirov SA, Fomitcheva IV, Sword J. Rapid neuronal ultrastructure disruption and recovery during spreading depolarization-induced cytotoxic edema. *Cereb Cortex*. 2020;30:5517–5531.
16. Cain SM, Bohnet B, LeDue J, *et al*. In vivo imaging reveals that pregabalin inhibits cortical spreading depression and propagation to subcortical brain structures. *Proc Natl Acad Sci USA*. 2017;114:2401–2406.
17. Van Harreveld A. Changes in volume of cortical neuronal elements during asphyxiation. *Am J Physiol*. 1957;191:233–242.
18. Van Harreveld A. Changes in the diameter of apical dendrites during spreading depression. *Am J Physiol*. 1958;192:457–463.
19. Kraig RP, Nicholson C. Extracellular ionic variations during spreading depression. *Neuroscience*. 1978;3:1045–1059.
20. Hossmann KA. Periinfarct depolarizations. *Cerebrovasc Brain Metab Rev*. 1996;8:195–208.
21. Dreier JP, Reiffurth C. Exploitation of the spreading depolarization-induced cytotoxic edema for high-resolution, 3D mapping of its heterogeneous propagation paths. *Proc Natl Acad Sci USA*. 2017;114:2112–2114.
22. Takano T, Tian GF, Peng W, *et al*. Cortical spreading depression causes and coincides with tissue hypoxia. *Nat Neurosci*. 2007;10:754–762.
23. Lauritzen M, Dreier JP, Fabricius M, Hartings JA, Graf R, Strong AJ. Clinical relevance of cortical spreading depression in neurological disorders: migraine, malignant stroke, subarachnoid and intracranial hemorrhage, and traumatic brain injury. *J Cereb Blood Flow Metab*. 2011;31:17–35.
24. Sugimoto K, Nomura S, Shirao S, *et al*. Cilostazol decreases duration of spreading depolarization and spreading ischemia after aneurysmal subarachnoid hemorrhage. *Ann Neurol*. 2018;84:873–885.
25. Dreier JP, Woitzik J, Fabricius M, *et al*. Delayed ischaemic neurological deficits after subarachnoid haemorrhage are associated with clusters of spreading depolarizations. *Brain*. 2006;129:3224–3237.
26. Dreier JP, Fabricius M, Ayata C, *et al*. Recording, analysis, and interpretation of spreading depolarizations in neurointensive care: Review and recommendations of the COSBID research group. *J Cereb Blood Flow Metab*. 2017;37:1595–1625.
27. Strong AJ, Fabricius M, Boutelle MG, *et al*. Spreading and synchronous depressions of cortical activity in acutely injured human brain. *Stroke*. 2002;33:2738–2743.
28. Escudero D, Valentin MO, Escalante JL, *et al*. Intensive care practices in brain death diagnosis and organ donation. *Anaesthesia*. 2015;70:1130–1139.
29. Johnston SC, Selvin S, Gress DR. The burden, trends and demographics of mortality from subarachnoid hemorrhage. *Neurology*. 1998;50:1413–1418.
30. Hartings JA, Andaluz N, Bullock MR, *et al*. Prognostic value of spreading depolarizations in patients with severe traumatic brain injury. *JAMA Neurol*. 2020;77:489–499.
31. Weidauer S, Lanfermann H, Raabe A, Zanella F, Seifert V, Beck J. Impairment of cerebral perfusion and infarct patterns attributable to vasospasm after aneurysmal subarachnoid hemorrhage: A prospective MRI and DSA study. *Stroke*. 2007;38:1831–1836.
32. Frontera JA, Claassen J, Schmidt JM, *et al*. Prediction of symptomatic vasospasm after subarachnoid hemorrhage: The modified Fisher scale. *Neurosurgery*. 2006;59:21–27. discussion 21–7.
33. van der Steen WE, Leemans EL, van den Berg R, *et al*. Radiological scales predicting delayed cerebral ischemia in subarachnoid hemorrhage: Systematic review and meta-analysis. *Neuroradiology*. 2019;61:247–256.
34. Saver JL. Time is brain–quantified. *Stroke*. 2006;37:263–266.
35. Carrera E, Schmidt JM, Oddo M, *et al*. Transcranial Doppler for predicting delayed cerebral ischemia after subarachnoid hemorrhage. *Neurosurgery*. 2009;65:316–323. discussion 323–4.
36. Vora YY, Suarez-Almazor M, Steinke DE, Martin ML, Findlay JM. Role of transcranial Doppler monitoring in the diagnosis of cerebral vasospasm after subarachnoid hemorrhage. *Neurosurgery*. 1999;44:1237–1247; discussion 1247–8.
37. Dreier JP, Major S, Lemale CL, *et al*. Correlates of spreading depolarization, spreading depression, and negative ultraslow potential in epidural versus subdural electrocorticography. *Front Neurosci*. 2019;13:373.
38. Dreier JP, Major S, Foreman B, *et al*. Terminal spreading depolarization and electrical silence in death of human cerebral cortex. *Ann Neurol*. 2018;83:295–310.
39. Busch E, Gyngell ML, Eis M, Hoehn-Berlage M, Hossmann KA. Potassium-induced cortical spreading depressions during focal cerebral ischemia in rats: contribution to lesion growth assessed by diffusion-weighted NMR and biochemical imaging. *J Cereb Blood Flow Metab*. 1996;16:1090–1099.
40. Takano K, Latour LL, Formato JE, *et al*. The role of spreading depression in focal ischemia evaluated by diffusion mapping. *Ann Neurol*. 1996;39:308–318.

41. Hadjikhani N, Sanchez Del Rio M, Wu O, *et al*. Mechanisms of migraine aura revealed by functional MRI in human visual cortex. *Proc Natl Acad Sci USA*. 2001;98:4687–4692.
42. Olesen J, Larsen B, Lauritzen M. Focal hyperemia followed by spreading oligemia and impaired activation of rCBF in classic migraine. *Ann Neurol*. 1981;9:344–352.
43. Lauritzen M, Skyhøj Olsen T, Lassen NA, Paulson OB. Changes in regional cerebral blood flow during the course of classic migraine attacks. *Ann Neurol*. 1983;13:633–641.
44. Major S, Huo S, Lemale CL, *et al*. Direct electrophysiological evidence that spreading depolarization-induced spreading depression is the pathophysiological correlate of the migraine aura and a review of the spreading depolarization continuum of acute neuronal mass injury. *Geroscience*. 2020;42:57–80.
45. Sadeghian H, Lacoste B, Qin T, *et al*. Spreading depolarizations trigger caveolin-1-dependent endothelial transcytosis. *Ann Neurol*. 2018;84:409–423.
46. Kors EE, Terwindt GM, Vermeulen FL, *et al*. Delayed cerebral edema and fatal coma after minor head trauma: Role of the CACNA1A calcium channel subunit gene and relationship with familial hemiplegic migraine. *Ann Neurol*. 2001;49:753–760.
47. Dreier JP, Jurkat-Rott K, Petzold GC, *et al*. Opening of the blood-brain barrier preceding cortical edema in a severe attack of FHM type II. *Neurology*. 2005;64:2145–2147.
48. Carlson AP, Shuttleworth CW, Major S, Lemale CL, Dreier JP, Hartings JA. Terminal spreading depolarizations causing electrocortical silencing prior to clinical brain death: case report. *J Neurosurg*. 2019;131:1773–1779.
49. Dreier JP, Reiffurth C. The stroke-migraine depolarization continuum. *Neuron*. 2015;86:902–922.
50. Hartings JA, Shuttleworth CW, Kirov SA, *et al*. The continuum of spreading depolarizations in acute cortical lesion development: Examining Leao's legacy. *J Cereb Blood Flow Metab*. 2017;37:1571–1594.
51. von Bornstädt D, Houben T, Seidel JL, *et al*. Supply-demand mismatch transients in susceptible peri-infarct hot zones explain the origins of spreading injury depolarizations. *Neuron*. 2015;85:1117–1131.
52. Somjen GG. Mechanisms of spreading depression and hypoxic spreading depression-like depolarization. *Physiol Rev*. Jul 2001;81:1065–1096.
53. Nozari A, Dilekoz E, Sukhotinsky I, *et al*. Microemboli may link spreading depression, migraine aura, and patent foramen ovale. *Ann Neurol*. 2010;67:221–229.
54. Dreier JP, Kleeberg J, Petzold G, *et al*. Endothelin-1 potently induces Leao's cortical spreading depression in vivo in the rat: A model for an endothelial trigger of migrainous aura? *Brain*. 2002;125:102–112.
55. Dreier JP, Korner K, Ebert N, *et al*. Nitric oxide scavenging by hemoglobin or nitric oxide synthase inhibition by N-nitro-L-arginine induces cortical spreading ischemia when K^+ is increased in the subarachnoid space. *J Cereb Blood Flow Metab*. 1998;18:978–990.
56. Tamim I, Chung DY, de Morais AL, *et al*. Spreading depression as an innate antiseizure mechanism. *Nat Commun*. 2021;12:2206.
57. Dreier JP, Isele T, Reiffurth C, *et al*. Is spreading depolarization characterized by an abrupt, massive release of Gibbs free energy from the human brain cortex? *Neuroscientist*. 2013;19:25–42.
58. Piilgaard H, Lauritzen M. Persistent increase in oxygen consumption and impaired neurovascular coupling after spreading depression in rat neocortex. *J Cereb Blood Flow Metab*. 2009;29:1517–1527.
59. Skou JC, Esmann M. The Na, K-ATPase. *J Bioenerg Biomembr*. 1992;24(3):249–261.
60. Shuttleworth CW, Andrew RD, Akbari Y, *et al*. Which spreading depolarizations are deleterious to brain tissue? *Neurocrit Care*. 2020;32:317–322.
61. Gathier CS, van den Bergh WM, van der Jagt M, *et al*. Induced hypertension for delayed cerebral ischemia after aneurysmal subarachnoid hemorrhage: A randomized clinical trial. *Stroke*. 2018;49:76–83.
62. Carlson AP, Abbas M, Alunday RL, Qeadan F, Shuttleworth CW. Spreading depolarization in acute brain injury inhibited by ketamine: A prospective, randomized, multiple crossover trial. *J Neurosurg*. Published online 25 May 2018. doi:10.3171/2017.12.JNS171665
63. Santos E, Olivares-Rivera A, Major S, *et al*. Lasting s-ketamine block of spreading depolarizations in subarachnoid hemorrhage: A retrospective cohort study. *Crit Care*. 2019;23:427.
64. Dreier JP, Major S, Manning A, *et al*. Cortical spreading ischaemia is a novel process involved in ischaemic damage in patients with aneurysmal subarachnoid haemorrhage. *Brain*. 2009;132:1866–1881.
65. Etminan N, Vergouwen MDI, Ilodigwe D, Macdonald RL. Effect of pharmaceutical treatment on vasospasm, delayed cerebral ischemia, and clinical outcome in patients with aneurysmal subarachnoid hemorrhage: A systematic review and meta-analysis. *J Cereb Blood Flow Metab*. 2011;31:1443–1451.
66. Hanley JA, McNeil BJ. The meaning and use of the area under a receiver operating characteristic (ROC) curve. *Radiology*. 1982;143:29–36.
67. Weidauer S, Vatter H, Beck J, *et al*. Focal laminar cortical infarcts following aneurysmal subarachnoid haemorrhage. *Neuroradiology*. 2008;50:1–8.
68. Dreier JP, Sakowitz OW, Harder A, *et al*. Focal laminar cortical MR signal abnormalities after subarachnoid hemorrhage. *Ann Neurol*. 2002;52:825–829.
69. Neil-Dwyer G, Lang DA, Doshi B, Gerber CJ, Smith PW. Delayed cerebral ischaemia: the pathological substrate. *Acta Neurochir*. 1994;131:137–145.
70. Schatlo B, Dreier JP, Gläsker S, *et al*. Report of selective cortical infarcts in the primate clot model of vasospasm after subarachnoid hemorrhage. *Neurosurgery*. 2010;67:721–728. discussion 728–9.
71. Stoltenburg-Didinger G, Schwarz K. Brain lesions secondary to subarachnoid hemorrhage due to ruptured aneurysms. In: Cervós-Navarro J, Ferszt R, eds. *Stroke and microcirculation*. Raven Press; 1987:471–480.
72. Vergouwen MD, Algra A, Rinkel GJ. Endothelin receptor antagonists for aneurysmal subarachnoid hemorrhage: A systematic review and meta-analysis update. *Stroke*. 2012;43:2671–2676.
73. Woitzik J, Dreier JP, Hecht N, *et al*. Delayed cerebral ischemia and spreading depolarization in absence of angiographic vasospasm after subarachnoid hemorrhage. *J Cereb Blood Flow Metab*. 2012;32:203–212.
74. Vergouwen MDI, Etminan N, Ilodigwe D, Macdonald RL. Lower incidence of cerebral infarction correlates with improved functional outcome after aneurysmal subarachnoid hemorrhage. *J Cereb Blood Flow Metab*. 2011;31:1545–1553.
75. Hecht N, Schrammel M, Neumann K, *et al*. Perfusion-dependent cerebral autoregulation impairment in hemispheric stroke. *Ann Neurol*. 2021;89:358–368.
76. Bosche B, Graf R, Ernestus RI, *et al*. Recurrent spreading depolarizations after subarachnoid hemorrhage decreases

oxygen availability in human cerebral cortex. *Ann Neurol*. 2010;67:607–617.
77. Hatashita S, Hoff JT, Salamat SM. Ischemic brain edema and the osmotic gradient between blood and brain. *J Cereb Blood Flow Metab*. 1988;8:552–559.
78. Hatashita S, Hoff JT. Brain edema and cerebrovascular permeability during cerebral ischemia in rats. *Stroke*. 1990;21:582–588.
79. Yang GY, Betz AL. Reperfusion-induced injury to the blood-brain barrier after middle cerebral artery occlusion in rats. *Stroke*. 1994;25:1658–1664. discussion 1664–5.
80. Dietrich WD, Busto R, Watson BD, Scheinberg P, Ginsberg MD. Photochemically induced cerebral infarction. II. Edema and blood-brain barrier disruption. *Acta Neuropathol*. 1987;72:326–334.
81. Woitzik J, Hecht N, Pinczolits A, *et al*. Propagation of cortical spreading depolarization in the human cortex after malignant stroke. *Neurology*. 2013;80:1095–1102.
82. Schoknecht K, Kikhia M, Lemale CL, *et al*. The role of spreading depolarizations and electrographic seizures in early injury progression of the rat photothrombosis stroke model. *J Cereb Blood Flow Metab*. 2021;41:413–430.